Genetically redirected HBV-specific T cells target HBsAg-positive hepatocytes and primary lesions in HBV-associated HCC

Xueshuai Wan[1], Karin Wisskirchen[2], Tao Jin[2], Lu Yang[2], Xiaorui Wang[2], Xiang'an Wu[1], Fang Liu[1], Yu Wu[1], Christy Ma[2], Yong Pang[2], Qi Li[2], Ke Zhang[2], Ulrike Protzer[3], Shunda Du[1]

[1] Department of Liver Surgery, Peking Union Medical College Hospital, PUMC, and Chinese Academy of Medical Sciences

[2] SCG Cell Therapy Pte. Ltd.

[3] Institute of Virology, School of Medicine, Technical University of Munich / Helmholtz Munich, Munich, Germany.

Corresponding authors:

Scientific background: Prof. Dr. Ulrike Protzer (Orcid ID 0000-0002-9421-1911)

Institute of Virology
Technical University of Munich /Helmholtz Munich
Trogerstrasse 30,
81675 Munich, Germany
Tel: 49-89-4140 6821
Fax: 49-89-4140 6823
E-mail: protzer@tum.de

Clinical application: Prof. Dr. Shunda Du (Orcid ID 0000-0002-9357-3259)

Department of Liver Surgery,
Peking Union Medical College Hospital, Chinese Academy of Medical Sciences and Peking Union Medical College
1 Shuaifuyuan, Wangfujing,
Beijing 100730, P. R. China
Tel: 86-10-69152836
Fax: 86-10-69156043
E-mail: dushd@pumch.cn

Running title:

T-cell therapy of HBV-HCC

Abbreviations:

ACT Adoptive cell therapy
AFP Alpha-fetoprotein
ALT Alanine aminotransferase
AST Aspartate aminotransferase
BCLC Barcelona Clinical Liver Cancer
CAR Chimeric antigen receptor
CBA Cytokine Bead Array
CCR C-C chemokine receptor
CD Cluster of differentiation
CHB Chronic hepatitis B
CRP C-reactive protein
CRS Cytokine release syndrome
Cy/Flu Cyclophoshphamide plus Fludarabine
CT Computer-assisted tomography
DLT Dose-limit toxicity
DNA Deoxyribonucleic acid
E:T Effector to target ratio
ECOG Eastern Cooperative Oncology Group
GMP Good Manufacturing Practice
Gt Genotype
HBcAg Hepatitis B core antigen
HBeAg Hepatitis B e antigen
HBsAg Hepatitis B surface antigen
HBV Hepatitis B virus
HBV-DNA Deoxyribonucleic acid of hepatitis B virus
HCC Hepatocellular carcinoma
HLA Human leukocyte antigen
IFN-γ Interferon-gamma
IHC Immunohistochemistry
IL Interleukin
INR International normalized ratio
iRECIST Immune Response Evaluation Criteria in Solid Tumors
IV Intravenous
LD Lymphodepletion
LHD Lactate dehydrogenase
MHC Major Histocompatibility Complex

mRECIST Modified Response Evaluation Criteria in Solid Tumors
mTRAC Minimally murinized T cell receptor constant region α-chain
mTRBC Minimally murinized T cell receptor constant region β-chain
NPG NOD-Cg-PrkdcSCIDIL-2Rgcnull/vst
PBMCs Peripheral blood mononuclear cells
PD-1 Programmed cell death protein 1
PR Partial response
qPCR Quantitative polymerase chain reaction
RNA Ribonucleic acid
RTCA Real time cell analysis
SAE Serious adverse event
S20 Amino acid position 20 of the HBV S protein
TCR T cell receptor
TCR-T T cell receptor T cells
TNF-α Tumor necrosis factor-α
TRAE Treatment related adverse event
TRAV T cell receptor variable region α-chain
TRBV T cell receptor variable region β-chain
ULN Upper limit of normal

Abstract

Background and Aims: HBV-DNA integration in HBV-related hepatocellular carcinoma (HBV-HCC) can be targeted by HBV-specific T cells. SCG101 is an autologous, HBV-specific T-cell product expressing a T-cell receptor (TCR) after lentiviral transduction recognizing the envelope-derived peptide (S_{20-28}) on HLA-A2. We here validated its safety and efficacy preclinically and applied it in an HBV-related HCC patient (NCT05339321).

Methods: GMP-grade manufactured cells were assessed for off-target reactivity and functionality against hepatoma cells. Subsequently, a patient with advanced HBV-HCC (Child-Pugh:A, BCLC:B, ECOG:0, HBeAg-, serum HBsAg+, hepatocytes 10% HBsAg+) received $7.9x10^7$ cells/kg after lymphodepletion. Safety, T-cell persistence, and antiviral and antitumor efficacy were evaluated.

Results: SCG101, produced at high numbers in a closed-bag system, showed HBV-specific functionality against HBV-hepatoma cells *in vitro* and *in vivo*. Clinically, treatment was well tolerated, and all adverse events, including transient hepatic damage, were reversible. On day 3, ALT levels increased to 1404 U/ml, and concurrently, serum HBsAg started decreasing by 3.84log and remained <1 IU/ml for over six months. HBsAg expressing hepatocytes in liver biopsies were undetectable after73 days. The patient achieved a partial response according to mRECIST score with a >70% reduction of target lesion size. Transferred T cells expanded, developed a stem cell-like memory phenotype, and were still detectable after six months in the patient's blood.

Conclusions: SCG101 T-cell therapy showed encouraging efficacy and safety in pre-clinical models and in a patient with primary HBV-HCC and concomitant chronic hepatitis B with the

capability to eliminate $HBsAg^+$ cells and achieve sustained tumor control after single dosing.

Keywords:

HBV-induced HCC, adoptive cell therapy, chronic hepatitis B, immunotherapy, T cell receptor

Highlights:

- Patient-derived T cells can be manufactured via lentiviral transduction under GMP conditions to express an HBV-specific TCR.
- HBV-specific T cells did not elicit off-target toxicity *in vitro, in vivo*, and in a patient suffering from an HBV-related HCC.
- HBV-specific T cells persist after single dosing in the HBV-HCC patient, resulting in robust HBsAg reduction and reduction of tumor lesions by >70%.

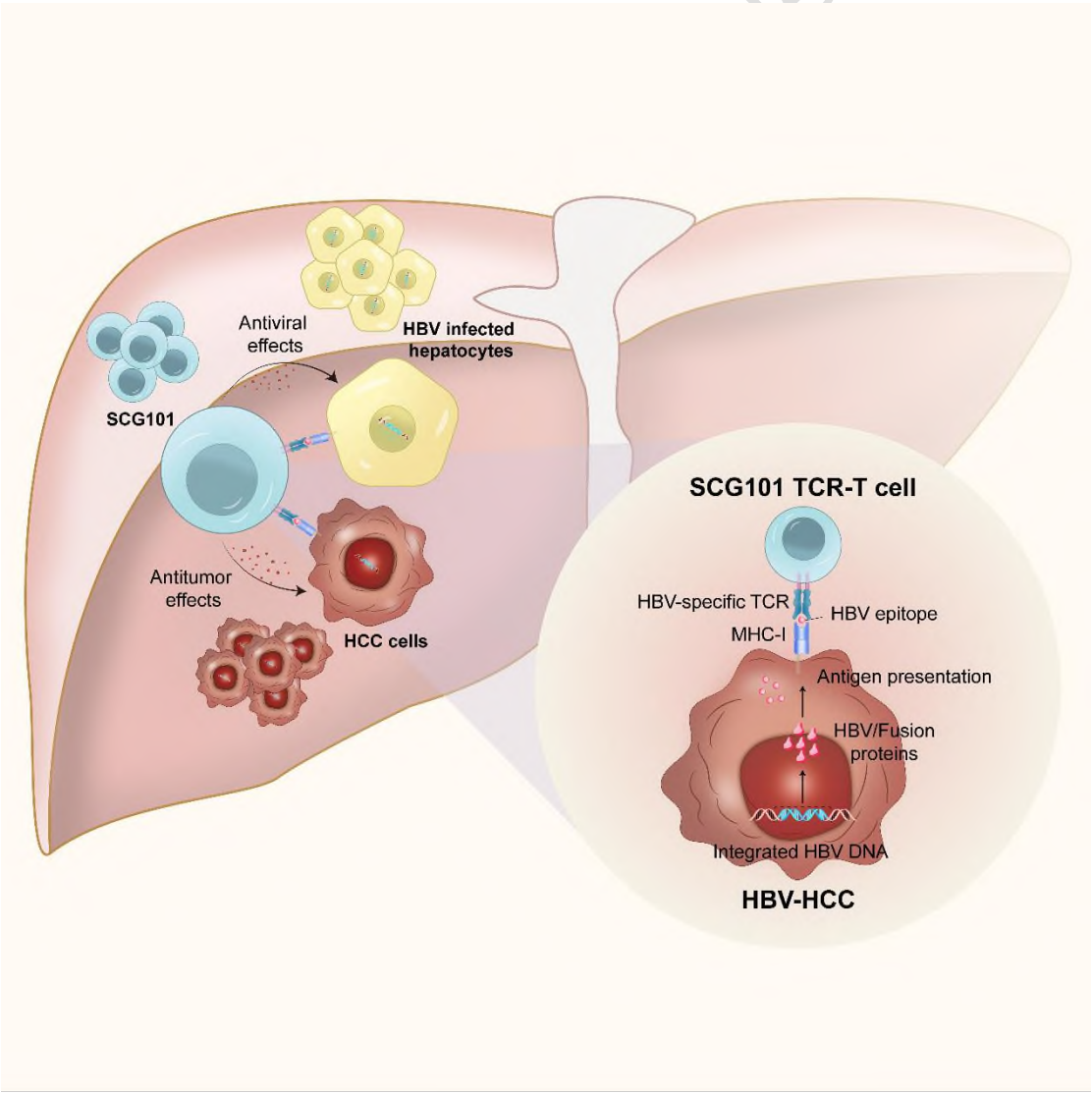

127 **Introduction**

128 Hepatocellular carcinoma (HCC) is the sixth most common malignancy and the third leading
129 cause of cancer-related mortality worldwide.[1] Systemic HCC therapies encompass immune
130 checkpoint, angiogenesis, or tyrosine kinase inhibitors, but response rates remain limited.[2] The
131 risk of HCC recurrence is high because the therapies do not target the underlying cause of HCC
132 development.

133 Hepatitis B virus (HBV) infection is the primary risk factor for HCC development, accounting
134 for ~50% of HCC worldwide and ~85% in China.[3] Despite the implementation of vaccination
135 programs, the projected number of liver cancer cases in China remains high, with 300,000 total
136 cases predicted for 2030[3] HBV-DNA integration is detected in 86% of HBV-related HCC tumor
137 cells.[4] HBV-DNA integration contributes to tumorigenesis and can result in persistent
138 expression of either complete HBsAg or fragments thereof depending on the integration sites.
139 This renders HBsAg an interesting therapeutic target as HBsAg is clearly distinct from proteins
140 expressed in healthy liver tissue. As such, it represents an ideal target for adoptive T-cell (ACT)
141 of HBV-related HCC, as it is also able to address the underlying cause of HCC development.
142 Clonal expansion of hepatocytes with HBV-DNA integration occurs early after infection and
143 increases with disease progression.[5,6] Consequently, targeting these potentially premalignant
144 cells seems crucial to prevent further HCC progression and the formation of new lesions.

145 HBV breakpoints resulting in HBV-DNA integration most commonly localize within an 1800
146 bp region of the HBV genome, preserving the structural integrity of the envelope, X and
147 polymerase open reading frames.[4] In advanced stages of chronic hepatitis B (CHB) and HCC,
148 a substantial proportion of HBsAg appears to emanate from integrated DNA rather than from

149 active viral infection[7], and particularly ground glass hepatocytes contain abundant HBsAg.[8] The
150 number of $HBsAg^+$ cells determined by histological staining is variable, ranging from 8-42 %
151 within tumor tissue and 71-86% in adjacent non-tumor tissue.[9–12] Even in histologically
152 negative HCC samples, HBsAg RNA can be detected via qPCR and Nanostring technology.[13]
153 Immunopeptidomics analysis of HBV-HCC samples confirmed that most of the HBV peptides
154 presented on tumor cells are derived from envelope and polymerase proteins.[14,15] HBV peptide
155 S_{20} (also referred to as Env_{183}) was presented on HLA-A*02 in HCC samples and in adjacent
156 non-tumorous liver tissue.[14,15] T cells genetically modified to express HBV-specific TCRs can
157 be redirected to recognize HBV-positive target cells.[16,17] Out of a library of HBV-specific TCRs,
158 a most sensitive and highly specific, HLA-A*02-restricted TCR recognizing the HBV S20
159 peptide was selected for preclinical and clinical development.[17] T cells expressing this HBV-
160 specific TCR secrete pro-inflammatory and antiviral cytokines, and electively eliminate HBV-
161 positive hepatoma cells and HBV-infected target cells, thereby clearing viral infection.[18]
162 In earlier clinical studies, T cells transiently expressing an HBV-specific TCR after RNA-
163 electroporation were used to target HBV-HCC metastases[13] In that setting, HLA-A2-restricted,
164 HBV-specific T cells were repeatedly applied to patients that had been transplanted with an
165 HLA-mismatched liver, thereby only targeting metastases of the original tumor but not the
166 transplanted liver.[13] Given the mere mass of malignant cells within a solid tumor such as an
167 HCC, we hypothesized that tumor targeting and efficient killing of tumor cells would require a
168 stable expression of an HBV-specific TCR to allow T-cells to expand while maintaining their
169 specificity and effector function. Therefore, a GMP-compliant, semi-automated protocol for
170 generating and upscaling an autologous T-cell product by lentiviral transduction and expansion

171 was developed. Functionality and safety of the HBV-specific TCR T cell product (product code
172 SCG101) were evaluated in preclinical models. Furthermore, for the first time, these stably
173 TCR-expressing autologous cells were studied in a setting of primary HBV-related HCC and
174 concomitant chronic hepatitis B. We here report the application of a single dose of SCG101 in
175 an HLA-A*02:01-positive patient within an investigator-initiated clinical trial (NCT05339321).
176

177 **Material & Methods**

178 **T-cell transduction**

179 The patient´s peripheral blood mononuclear cells were collected by leukocyte apheresis. Cells
180 were sorted by magnetic beads carrying CD4 and CD8 antibodies (Miltenyi Biotec) on a
181 CliniMACS® Plus Instrument under good-manufacturing-practice (GMP) conditions.
182 Subsequently, the sorted $CD4^+$ and $CD8^+$ T cells were activated by Transact microspheres
183 presenting CD3 and CD28 antibodies (Miltenyi Biotec) and cultured in Prime-XV T-cell
184 medium (Irvine Scientific) with 400 IU/ml IL-2 (Shandong Quangang Co.).
185 A GMP-grade lentivirus (produced by WuXi AppTec.) encoding the HBsAg-specific TCR gene
186 was added to activated T cells on day 1. Cells were cultured at 37 °C for 8 to 12 days in a closed
187 bag system (Cytiva) on a Xuri Cell Expansion System W25 (Cytiva). Cells were harvested by
188 300xg centrifugation for 5 minutes at room temperature and then washed with a saline solution
189 containing 5 % human albumin (FLEXBUMIN, Baxter). After washing, cells were frozen in
190 CS10 medium (Stemcell) and stored at -150℃.

191 **T-cell functionality assays**

192 For cytokine production assays, $5x10^4$ T cells were co-cultured with an equal number of target

193 cells in 96-well U-bottom plates. Reactivity against the S20 HLA-A*02:01-presented peptide
194 was determined by pulsing T2 cells with peptide (1 μM, or as indicated) for two hours before
195 co-culture. Co-culture supernatants were harvested after 18–24 hours, and IFN-γ or TNF-α
196 concentrations were measured by Cytometric Bead Array (CBA, BD Biosciences) according to
197 the manufacturer´s instructions. Cytotoxicity assays were performed by co-culture of T cells
198 with target cells at the indicated effector-to-target (E:T) ratios. Briefly, $2x10^4$ target cells per
199 well were seeded and cultured overnight before effector T cells were added at the indicated
200 ratios. Target cell lysis was evaluated with the xCELLigence Real-Time Cell Analyzer (ACEA
201 Biosciences), which assessed electrical impedance due to the adherence of cells in each well
202 every 15 minutes until the end of the experiment. The data were processed using the
203 xCELLigence RTCA software, and the results are reported as a cell index value, which was set
204 to 1 when T cells were added.

205 **Patient characteristics and clinical intervention.**

206 The patient described herein provided written informed consent to be enrolled in an
207 investigator-initiated study (NCT05339321). The protocol was approved by the local ethics
208 committee of the Peking University Cancer Hospital. The study was conducted in accordance
209 with the International Conference on Harmonization Guidelines for Good Clinical Practice and
210 the Declaration of Helsinki. The patient received compensation for travel and a meal per visit.
211 The primary objective of this study was to assess the safety and tolerability of SCG101 in HCC
212 patients who were serum HBsAg positive, HBeAg negative, and had HBV-DNA levels ≤
213 2×10^3 IU/ml, were HLA-A*02 positive and had failed at least two prior lines of treatment.
214 The enrolled participant presented here was an HBeAg-negative individual with an HBsAg

215 level of 651 IU/ml during the screening phase. He was genotyped as HLA-A*02:01 and
216 categorized as Child-Pugh A based on liver function assessment. Before intravenous infusion
217 of SCG101, the patient received lymphodepletion chemotherapy (fludarabine 25 mg/m^2/day
218 and cyclophosphamide 500 mg/m^2/day on days -6 to -4) for preconditioning. On day 0, the
219 subject received 7.9x10^7 TCR-T cells per kg, corresponding to 5.9×10^9 total TCR-T cells. Cell
220 infusion took 70 minutes.
221 Efficacy was evaluated according to modified RECIST (mRECIST and iRECIST) criteria.
222 Imaging and tumor assessment were conducted in month one, month two, and every two months
223 thereafter by computed tomography (CT) using a contrast agent.
224 **Biopsy staining**
225 Liver biopsies were formalin-fixed and paraffin-embedded before 4 μm tissue sections were
226 obtained. Immunohistochemistry (IHC) staining using the BOND RX Fully Automated
227 Research Stainer (Leica) with a bond polymer refine DAB detection. Deparaffinized slides were
228 incubated with anti-HLA-A (#ab52922, Abcam), anti-HBcAg (#CHM-0100, CELNOVTE,
229 China) or anti-HBsAg (#CHM-0121, CELNOVTE, China) antibody for 60 minutes and then
230 treated with anti-polymer peroxidase-conjugated (HRP) secondary antibody (#DS9800, Leica)
231 for 30 minutes. Slides were then treated with Hematoxylin, washed in distilled water, counter-
232 stained with Eosin and manually covered. Slides were air-dried and mounted with an anti-fade
233 mounting medium, and pictures were taken on a Pannoramic Midi II system (3DHistech Ltd.).
234

235 **Results**

236

237 **Specificity of the clinical T-cell product SCG101**

238 SCG101 is a human TCR T-cell product expressing a natural, high-affinity TCR isolated from
239 an HLA-A*02:01^{+} donor with resolved HBV infection[17] The TCR construct comprised V alpha
240 34 and V beta 5.1 variable domains fused to minimally-murinized cysteine-modified constant
241 domains to enhance correct pairing of the TCR chains while keeping immunogenicity at a
242 minimum (Fig. 1A).[19] The TCR was cloned into a lentiviral vector for transduction of T cells
243 with a GMP-compliant protocol. As part of the cell product assessment before clinical
244 application, SCG101 T cells were characterized *in vitro* and in preclinical models.

245 Specific binding of the TCR to its peptide-MHC complex (S20 FLLTRILTI_HLA-A*02:01-
246 S20) was dose-dependent with a half-maximum binding activity of 2.1 nM (Fig. 1B). Within
247 primary SCG101 T cells, CD8^{+} as well as CD4^{+} T cells were able to bind the S20 multimer,
248 indicating a transduction rate of almost 90 % (Fig. 1C). Staining using an antibody specific to
249 the TCR beta chain Vβ5.1 and an HLA-A*02-S20 multimer allowed to estimate TCR
250 expression and pairing efficiency, respectively. Accordingly, TCR mispairing with endogenous
251 TCR sequences may be deduced from positive Vβ staining in the absence of multimer-binding.
252 The maximum likelihood of such mispairing was low, with a mean value of 7% among six
253 batches of SCG101 T cells (Fig. 1C).

254 To investigate the specific binding of SCG101 further, we aimed to assess critical amino acids
255 within the TCR epitope sequence that are either essential for recognition by SCG101 T cells or
256 for peptide binding to the HLA-A2 molecule. The exchange of L-T-R-I at position S22-S25 led

257 to a 90-99% reduced recognition of the peptide, indicating the potential binding motif (Fig. 1D).
258 Next, we assessed the cross-reactivity of SCG101 with human peptides and potential off-target
259 activity. Neither the nine human peptides identified to contain the potential binding motif L-T-
260 R-I (Fig. 1E, Fig. S1A) nor the 14 peptides that shared six identical amino acids with peptide
261 S20 (Fig. 1F, Fig. S1B) led to activation of SCG101 T cells. Hence, the results demonstrated
262 the specificity of SCG101´s TCR and indicated the absence of cross-reactivity against tested
263 very similar human peptides. Taken together, the SCG101 T cell product exhibited clearly
264 recognizable levels of TCR expression and correct TCR chain pairing while retaining
265 specificity to its cognate HBV peptide.
266

267 **Potency of SCG101 T cells**

268 We next asked whether the clinical-grade SCG101 T cell product produced using a new
269 upscaling protocol under GMP conditions would maintain antiviral and antitumor potency.[18]
270 The functional avidity of SCG101 was measured by secretion of pro-inflammatory cytokines
271 towards a dose-titration of peptide S20 loaded onto T2 cells compared to peptide C18, which
272 should not be recognized (Fig. 2A). IFN-γ secretion proved most sensitive with an EC_{50} of
273 $1.55x10^{-8}$ M. When co-cultured with $HBsAg^{+}$ HepG2 hepatoma cells, SCG101 T cells were
274 able to kill rapidly and specifically up to 100% of target cells within 48 hours (Fig. 2B).
275 Consistent with the cytotoxic capability of SCG101, the antiviral cytokine IFN-γ was produced
276 at high levels of 20 ng/ml upon antigen stimulation at an E:T of 1:1 (Fig. 2C). HBsAg was
277 reduced by approximately 50% within two days of co-culture (Fig. 2D).
278

279 ***In vivo* efficacy of SCG101 T cells**

280 To analyze the anti-tumor activity and tissue distribution of SCG101 in an *in vivo* model, we
281 used a xenograft model with transplanted $HBsAg^+$ hepatoma cells. When tumors had formed,
282 four different SCG101 dose levels ranging from 2 to 20 million TCR^+ T cells were applied (Fig.
283 3A). Animals did not lose body weight during treatment (Fig. 3B), and by day 21, tumor growth
284 inhibition in all SCG101 TCR-T groups was >95% (Fig. 3C).

285 The same preclinical model was also used to study the pharmacokinetics of the highest dose of
286 TCR^+ T cells (Fig. S2A). The distribution of SCG101 was analyzed by qPCR of 14 different
287 tissues at six consecutive time points over three weeks. After a single dose of $1x10^9$ TCR^+ T
288 cells/kg, the cells had rapidly distributed throughout the body by day one. After a gradual
289 decrease of SCG101 in all tissues by day seven, copy numbers increased again in the following
290 two weeks, peaking on day 21 (Fig. S2B), indicating T-cell expansion upon antigen recognition.
291 SCG101 accumulated mainly in the lung, spleen, blood, and liver (Fig S2C). Taken together,
292 SCG101 TCR-T mediated a high target-specific anti-tumor activity and initiated T-cell
293 persistence *in vivo*.

294

295 **Application of HBV-specific T cells in a clinical setting**

296 Encouraged by the preclinical data showing the anti-tumor activity of SCG101, an investigator-
297 initiated trial, "Clinical study of SCG101 in the Treatment of Subjects with Hepatitis B Virus-
298 Related Hepatocellular Carcinoma (SCG101-CI-101)", was set-up. It was approved by the local
299 ethics board. A 54-year-old HLA-A*02:01^+ man diagnosed with CHB and primary HCC in
300 2019 was enrolled in the study and infused with SCG101 in July 2022. The patient had a history

of tumor and liver segment VIII resection in 2019, followed by trans-arterial chemo-embolizations in 2019 and 2021 and Sorafenib treatment for one year. The patient started to take Entecavir for HBV infection management in March 2022 (Fig. 4A). The status of his liver disease was Child-Pugh score A, ECOG performance status 0, BCLC stage B and CNLC stage IIb without extrahepatic metastasis, portal vein thrombosis, or other comorbidities (Fig. 4B). An archived liver biopsy sample taken three months before adoptive T-cell transfer was analyzed (Fig. 4C). Despite having multiple nodules in two target lesions, obtaining a tumor biopsy was unsuccessful. Histological analysis revealed an intense HLA-A staining along sinusoids and a weaker HLA-A staining on hepatocytes (Fig. 4D). The tissue stained negative for HBcAg (Fig. 4E) and an average of around 10% of hepatocytes across three different sections stained positive for HBsAg (Fig. 4F).

After signing informed consent, the patient underwent leukapheresis to obtain PBMC to produce SCG101 with the standardized protocol under GMP conditions. The cell product contained 30% TCR^+ T cells, a $CD8^+$ to $CD4^+$ T-cell frequency of 62.12 % and 36.78 %, respectively (Fig. S3A), and passed all the quality controls and release criteria (Fig. S3B). The data cut-off was February 7, 2023.

Treatment-Related Events

One week before treatment, lymphodepletion was performed on three consecutive days using cyclophosphamide and fludarabine. Finally, a single dose of $7.9x10^7$ per kg corresponding to 5.9×10^9 total TCR-T cells was infused. Upon adoptive T-cell transfer, the patient was closely monitored for treatment-related adverse events (TRAE) and blood was analyzed regularly (Fig.

5A). The patient tolerated SCG101 therapy well, no treatment-related serious adverse events (SAEs), neurotoxicity, or infusion reactions occurred and all TRAEs were manageable and reversible (Table 1, Fig. S4). TRAEs of grade 3 or 4 included cytokine release syndrome (CRS), hypotension, cytopenia, ALT and AST increase (Table 1). Cytopenia, which was anticipated due to the Cy/Flu preconditioning, comprised a decrease in lymphocytes, monocytes, neutrophils, and total white blood cells (Table 1, Fig. S4A-D) and, in general, recovered to grade 2 within 30 days. However, a prolonged decrease and fluctuating platelet counts constituting grade 2 to grade 4 events were observed that finally resolved on D80 (Fig. S4E).

Since SCG101 can not only target the tumor but also infected hepatocytes, as observed in preclinical models[18] particular attention was given to the liver function. Pretreatment ALT was 18 U/L, the pretreatment international normalized ratio (INR) for blood clotting was 1, and the pretreatment bilirubin level was 14.0 μmol/L. ALT elevation after SCG101 infusion reached a peak of 1,404 U/L on day 3 (Fig. 5B), that of AST 1,140 U/L on day 2 (Fig. 5C), respectively, both constituting grade 4 events (Table 1). After liver protection therapy, including glutathione, diammonium glycyrrhizinate, ademetionine, and polyene phosphatidylcholine, ALT, AST, and lactate dehydrogenase (LDH, Fig. 5D) levels decreased gradually.

Elevation of liver enzymes was transient, returned to baseline on day 17, and was accompanied by a slight, transient increase in serum total bilirubin below two times the upper limit of normal (ULN) (Fig. 5E, S4G), ferritin (Fig 5E), creatinine and urea (Fig S4H,I), as well as a reduction in serum albumin below 35 g/L on a single day (Fig. 5G), while the INR remained normal (Fig. 5H).

After infusion of SCG101, a strong immune reaction followed, characterized by CRP, IL-6,

IFN-γ, IL-2, and IL-10 increasing rapidly one day after infusion (Fig. 5I-M, S4J), fever peaking at 39.8°C (Fig. S4L) and hypotension with a minimum blood pressure of 70/41 mmHg (Fig. S4M). The symptoms stabilized after antipyretic and symptomatic treatment with norepinephrine and rehydration. Together, these symptoms indicated a CRS and were contained with Tocilizumab and dexamethasone (10mg; 2x d1, 4x d2, 1x d3) and the subject started to recover by day three post-infusion. In summary, infusion of SCG101 induced non-serious side effects that were expected due to SCG101´s mode of action and were manageable with standard medication for immune-related events.

Expansion of HBV-specific T cells in peripheral blood

The efficacy of adoptive T-cell therapy in both liquid and solid tumors using gene-modified T cells is associated with the persistence of transferred cells[20,21]. We, therefore, analyzed this by flow cytometry and qPCR. *Ex vivo*, transferred T cells at peak expansion constituted around one-third of $CD3^+$ T cells in blood detected by flow cytometry (Fig. 6A) with a maximum of $4.37x10^4$/ml on day 21, suggesting a strong expansion (Fig. 6B). Both $CD8^+$ and $CD4^+$ HBV-specific TCR^+ T cells circulated equally as indicated by a slight increase in $CD4^+$ SCG101 T cells in blood compared to their proportion in the infusion product (Fig. 6B, S3A). Interestingly, while on day seven effector memory T cells ($CCR7^-CD45RA^-$) were still detected at equal numbers, mainly effector T cells ($CCR7^-CD45RA^+$) and T memory stem cells (T_{SCM}, $CCR7^+CD45RA^+$) circulated in peripheral blood thereafter within the first four weeks (Fig. 6C). HBV-specific T cells were able to persist at least until four months post transfer and by then almost exclusively consisted of T_{SCM} cells (Fig. 6C). Long-term survival of transferred

transduced T cells was confirmed by quantification of the copy number of the virus vector integrates (Fig. 6D). This analysis indicated a peak in viral-vector copies seven days post-transfer, stabilizing until day 21 and slowly dropping thereafter. Collectively, these data demonstrated an enduring persistence of engineered T cells circulating in the blood associated with the development and maintenance of a predominantly stem cell memory phenotype after antigen exposure.

Antiviral and antitumor activity of T cells redirected against HBsAg

Coinciding with the expansion of HBV-specific T cells and the increase in serum ALT, serum HBsAg substantially and rapidly decreased within one week after cell transfer from 557.96 to 1.3 IU/ml. The maximum reduction from baseline was 3.84 $\log_{10}$ to 0.08 IU/ml. It was maintained for more than six months (Fig. 7A). Serum HBV-DNA levels were low at baseline (29 IU/ml) and remained undetectable after cell infusion (Fig. 7B). Since no tumor tissue was contained in the biopsies obtained before treatment, the presence of the target on tumor cells remained unknown, and changes in HBsAg expression could only be analyzed in hepatocytes. Compared to the HBsAg expression in 10% of hepatocytes at screening (Fig. 4F), we barely observed HBsAg staining in hepatocytes by 73 days after cell infusion (Fig. 7C). AFP levels fluctuated and remained below 90 ng/ml until increasing again by day 133 (Fig. S4N).

At baseline, the subject presented with multiple nodules and two target lesions in the right lobe with a 38 and 21 mm diameter, respectively (Fig. 7D, upper row). By day 28 post SCG101 infusion, a large area of tumor necrosis was observed (Fig. 7D, 2nd row), followed by a partial response (PR) with the target tumor lesions decreasing by 74.5% in mRECIST and by 47.5%

in iRECIST, respectively. The patient maintained a stable disease for at least 6.9 months, suggesting clinical antiviral as well as antitumor activity of HBV-specific T cells.

Discussion

HBV infection is a main driver for the development of HCC, and the available treatment options are limited. We here show that autologous, HBV-specific T cells can be manufactured using lentiviral transduction of a high-affinity TCR under GMP conditions, persist over several months, are safe and functioning in the clinical setting of an HBV-HCC, and lead to a profound reduction in viral markers and tumor mass.

SCG101 carries a natural TCR isolated from an HLA-A*02:01 donor with resolved HBV infection[17] Hence, it had undergone negative selection against self-antigens within the thymus of the donor, and, not surprisingly, we did not observe any off-target activity in the patient. Although an alanine-substitution scan identified position five to be part of the TCR recognition motif, SCG101 was capable of recognizing the two most common HBV peptide variants FLLTRILTI (gtA,C,D) and FLLTKILTI (gtB). This cross-recognition could be explained by Arginine (R) and Lysine (K) as positively charged amino acids sharing more similar properties than Arginine and Alanine. Furthermore, preclinical toxicology and distribution studies were performed according to regulatory standards. However, these xenograft mouse models can only provide limited information since cytokines, chemokines, and receptors do not match between the human T-cell product and the murine recipient. Therefore, it is reassuring to know that T-cell transfer was also safe in a syngeneic mouse model when murine SCG101 T cells were injected into $HBV^{+}HLA\text{-}A2^{+}$ mice.[22]

Overall, the treatment was well-tolerated, all TRAE were reversible through symptomatic interventions, and neither SAE nor DLT occurred. Grade 3 CRS became evident by an elevation of IL-6, fever, and hypotension, which likely led to increased levels of CREA and UREA in the blood due to reduced renal blood perfusion. CRS was effectively managed with Tocilizumab, corticoids, and noradrenaline. Notably, in the treatment of CD19-malignancies, CRS typically occurs more than 24 hours after CAR-T-cell infusion.[23] However, in the case presented here, the onset of CRS was unexpectedly rapid, with elevated body temperature and high IL-6 levels observed as early as two hours after the infusion. Generally, it is assumed that IFN-γ released by activated T cells leads to IL-6 production in bystander cells such as macrophages.[24] Our *in vitro* experiments using real-time cytotoxicity measurement revealed that T-cell activation and target cell killing occurred immediately after the co-culture began. Potentially, in the patient, effector function of the T cells started immediately after infiltration into the tissue, and the significant number of liver-resident Kupffer cell macrophages may have contributed to the rapid onset of CRS.

All grade 4 events (cytopenia and increased ALT/AST levels) were expected to be a positive sign of response to treatment. Cytopenia was intended and most likely induced by the pre-conditioning Cy/Flu regimen, which has been associated with better T-cell engraftment and outcome in CD19 CAR-T treatment[25] The reasons why patients benefit from lymphodepletion prior to ACT are not fully understood, and co-depletion of regulatory cells[26] an increase of serum cytokines[27,28] and tolerization towards xenogeneic sequences[29] have been discussed. Cytopenia also comprised a low platelet count, which started already at screening before treatment. It might have been prolonged due to multiple factors, including lymphodepletion,

Tocilizumab, and the study drug's proliferation. We suppose that a more proactive use of recombinant human thrombopoietin or thrombopoietin receptor agonists can be considered to help platelet count recover under such circumstances.

The elevation in ALT/AST levels occurred concomitant with a substantial reduction in serum HBsAg and is in line with SCG101´s anti-tumor and anti-viral cytotoxicity demonstrated before.[18] Notably, in addition to targeting tumor cells, HBV-specific T cells also recognize and attack hepatocytes that express HBsAg or fragments thereof, either due to HBV infection or HBV-DNA integration,[18] which likely led to the transient increase in serum transaminases. The ALT levels in our patient reached the 35-fold ULN. This, however, did not result in hepatic dysfunction or severe hepatic damage but rather indicated tumor cell lysis, as evidenced by the absence of impaired liver synthetic function (bilirubin, albumin, or INR), the absence of specific symptoms such as jaundice or bleeding, and the transient nature of the flare.[30] Cytotoxicity directed towards non-tumor HBV^+ hepatocytes is inherently linked to an effective T-cell response, either naturally generated during acute hepatitis and viral clearance or artificially generated via transfer of immune cells.[31] Indeed, transient ALT flares that are host-induced, i.e., comprising an effective immune response, but not virus-induced, can be associated with favorable outcomes [30] and viral clearance.[32,33]

Nonetheless, the mitigation of excessive liver damage following adoptive T-cell transfer remains a priority. To address this, inclusion required a Child-Pugh score ≤ 7 and ECOG performance status of 0 or 1 as well, and pre-treatment biopsies were analyzed for $HBsAg^+$ hepatocytes. Several studies have examined CHB patient biopsies to determine the frequency of $HBsAg^+$ hepatocytes with high variation from 0% to 100%,[34–39] with particularly high levels

when ground glass hepatocytes are present.[37] The most recent and comprehensive study by Aggarwal et al. analyzed biopsies from 114 patients, finding the average number of HBsAg^{+} hepatocytes to be below 10%. Interestingly, they observed a lack of correlation between quantification results from two biopsies collected from the same individual and time point.[36] This aligns with our findings of heterogenic HBsAg staining for subject ST1206, suggesting that multiple biopsies may be necessary to yield reliable results representing the entire liver. This information could be complemented by serum HBsAg levels, which generally, though not always,[34] correlate with intrahepatic HBsAg levels.[40] Additionally, more sophisticated probe-[13] or sequencing-based[41] assays might be necessary to assess the presence of the target peptide expressed from chimeras of HBV and host-cell nucleic acids that might not cover the full HBsAg open reading frame and might not be detectable by antibody staining.[13] We anticipate insights from the ongoing phase I/II study of SCG101 (NCT05417932) will contribute to identifying a reliable biomarker for safe patient stratification.

The patient described here was negative for HBcAg liver staining, HBeAg, and HBV-DNA, leading to the assumption that most of the serum HBsAg originated from tumor cells and/or hepatocytes with HBV-DNA integration rather than from active infection. Studies have indicated that HBsAg and HBcAg rarely colocalize in biopsy samples [9,36] and that in late-stage CHB, integrated HBV-DNA is the main source for HBsAg production.[42–44] HBsAg decline is the hallmark of effective anti-HBV treatment [45] and has not been achieved by RNA-interference-based therapies,[46] likely due to integrated HBV-DNA being the source of HBsAg.[47] Therefore, targeting integrated HBV-DNA has been suggested to be a goal in drug development.[48,49] With SCG101 treatment, we observed a considerable reduction in HBsAg,

approaching the detection limit of the diagnostic assay, which would have constituted a functional cure. Over six months, HBsAg levels did not rebound but were also not eliminated despite SCG101 persistence, and several reasons for this observation can be discussed. First, it is possible that HBsAg^{+} cells developed evasion strategies, such as HLA-loss or mutations in the peptide presentation pathway, similar to what has been observed in HPV-cancer patients refractory to treatment with HPV-specific T cells.[50] Second, SCG101 cells might have undergone similar exhaustion mechanisms as endogenous HBV-specific T cells in the liver and tumor.[51,52] Due to the limited amount of blood available for analysis, we were unfortunately unable to address this hypothesis. Although SCG101 T cells were still circulating in the blood after several months, we have no proof that they retained their functionality. However, in mice transduced with AAV-HBV and AAV-HLA-A2, we observed the same kinetics of ALT increase, HBsAg reduction, and persistence of HBV-specific T cells. Also, a residual low amount of HBsAg remained detectable in this syngeneic mouse model. When T cells were analyzed *ex vivo*, the high-avidity TCR-T cells could no longer be specifically activated by their cognate peptide.[22]

Most importantly, following activation of SCG101 in subject ST1206, a sizable and sustained antitumor effect was observed 28 days after cell infusion, lasting at least until the cut-off date. While tumor shrinkage occurred directly after SCG101 infusion, without a pre-treatment tumor biopsy, we can only speculate but not prove its direct cytotoxicity on tumor cells. Alternatively, an indirect effect can be envisioned, where SCG101 cells create an inflammatory environment, helping endogenous immune cells attack the tumor. This idea was already proposed when two patients treated with RNA-electroporated TCR-T cells experienced clear shrinkage of the primary tumor[53,54] or metastases[13]. Using mRNA, anti-tumor responses occurred only after

several infusions and during a time frame when the transferred cells most likely had lost their designed antigen-specificity due to the transient HBV-TCR expression after mRNA electroporation, while still other immunological alterations were detected.[13,54]

Notably, four months after T-cell infusion, a moderate rise in AFP levels was observed in our patient, exceeding pre-infusion levels. This AFP increase could indicate liver regeneration, as similar AFP rises have been observed in acute hepatitis B and correlated positively with the extent of transaminase elevation.[55,56] However, in this study, peak transaminase levels were followed by the AFP increase only four weeks later. Another potential hypothesis for the increase in AFP is that eliminating $HBsAg^{+}$ tumor and premalignant cells created space for HCC cells negative for the S20 target peptide of SCG101 to proliferate. Mason *et al.* proposed the "loss of productive HBV infection, providing at least partial escape from the antiviral immune response as a major facilitator of clonal expansion".[6] Given the early emergence of clonal growth,[5] we would expect this postulated negative effect of an antiviral immune response to also manifest in an increased number of HCC cases after spontaneous clearance in late-stage CHB. However, further investigations in larger cohorts are required to gather more data on this phenomenon.

The on-target efficacy observed with our selected dose of SCG101 and treatment scheme exceeded similar - albeit different - regimens using HBV-specific T cells transiently expressing a TCR after electroporation[13,53]. In patients with the indication of HBV-HCC-derived metastases and an HLA-A2- and/or HBV-negative liver after transplantation[13,57]HBsAg was reduced by almost 50% in 2/8 patients three to six months after infusing several doses of transient, RNA-electroporated TCR T cells[53] or by 90% in a single patient one month after

infusion of stably transduced TCR-T cells.[57] Although it is difficult to quantitatively compare these approaches due to different clinical settings, cell doses and duration of cellular functionality, it was remarkable that in the pioneering study of Qasim *et al*., the stably transduced TCR-T seemed to act faster and more efficiently despite a low transduction rate and a low dose of cells infused.[57]

This encouraged us to set up a highly efficient GMP-compliant transduction process generating higher TCR-T numbers that - as demonstrated in this study - after infusion quickly reduced HBsAg by 99.99%. Along with the stable expression of the TCR, other factors might have contributed to the clinical efficacy of SCG101. Its dual functionality in $CD8^+$ and $CD4^+$ T cells, the balance of both T-cell subtypes, and the shift to a memory stem cell phenotype might have supported the persistence and extended functionality of transferred T cells. A well-balanced CD8:CD4 T-cell ratio and the occurrence of the T_{SCM} phenotype have positively impacted the outcome of CAR-T therapy.[58–60] Potentially, also the encounter of HBsAg on hepatocytes may have facilitated the stimulation and expansion of transferred, stably TCR-expressing T cells before encountering the immunosuppressive tumor microenvironment. Others currently follow the same principle of using an RNA-vaccine to boost transferred claudin-specific CAR T cells to treat solid tumors.[61]

Overall, SCG101 presented as a safe product with its stable TCR expression, leading to both antitumor and antiviral effector functions and sustained persistence in the patient. Further studies will determine whether adoptive T-cell therapy can maintain a favorable risk-benefit ratio and has the potential to be applied to target the cause of malignant transformation to prevent additional tumor development.

Conflict of interest statement

KW, JT, LY, XiWa, YP, QL, CM and KZ are employees of SCG Cell Therapy; KZ and UP are board members of SCG Cell Therapy; KW, KZ, CM, and UP hold shares in SCG Cell Therapy Pte. Ltd. The other authors declare no conflict of interest.

Financial support

This study was supported by SCG Cell Therapy Pte. Ltd., and the Deutsche Forschungsgemeinschaft (DFG, German Research Foundation) via SFB-TRR 338/1 2021–452881907 to UP.

Author contributions

TJ and LY prepared preclinical experiments; SD and CM designed the clinical study; XuWa, XiWu, FL, and YW performed T-cell transfer and follow-up treatment; KW, XiWa, YP and QL analyzed data; KW wrote the manuscript; KZ, UP, and SD interpreted data and critically revised the manuscript.

References

1. Sung H, Ferlay J, Siegel RL, Laversanne M, Soerjomataram I, Jemal A, et al. Global Cancer Statistics 2020: GLOBOCAN Estimates of Incidence and Mortality Worldwide for 36 Cancers in 185 Countries. Ca Cancer J Clin. 2021;71:209–49.

2. Zhang H, Zhang W, Jiang L, Chen Y. Recent advances in systemic therapy for hepatocellular carcinoma. Biomark Res. 2022;10:3.

3. Zheng R, Qu C, Zhang S, Zeng H, Sun K, Gu X, et al. Liver cancer incidence and mortality in China: Temporal trends and projections to 2030. Chin J Cancer Res. 2018;30:571–9.

4. Sung WK, Zheng H, Li S, Chen R, Liu X, Li Y, et al. Genome-wide survey of recurrent HBV integration in hepatocellular carcinoma. Nat Genet. 2012;44:765–9.

5. Tu T, Mason WS, Clouston AD, Shackel NA, McCaughan GW, Yeh MM, et al. Clonal expansion of hepatocytes with a selective advantage occurs during all stages of chronic hepatitis B virus infection. J Viral Hepatitis. 2015;22:737–53.

6. Mason WS, Jilbert AR, Litwin S. Hepatitis B Virus DNA Integration and Clonal Expansion of Hepatocytes in the Chronically Infected Liver. Viruses. 2021;13:210.

7. Ringlander J, Andersson ME, Prakash K, Larsson SB, Lindh M. Deep sequencing of hepatitis B virus using Ion Torrent fusion primer method. J Virol Methods. 2022;299:114315.

8. Su I, Wang H, Wu H, Huang W. Ground glass hepatocytes contain pre-S mutants and represent preneoplastic lesions in chronic hepatitis B virus infection. J Gastroenterol Hepatol. 2008;23:1169–74.

9. Zheng Y, Xu M, Zeng D, Tong H, Shi Y, Feng Y, et al. In situ analysis of hepatitis B virus (HBV) antigen and DNA in HBV-induced hepatocellular carcinoma. Diagn Pathol. 2022;17:11.

10. Wang Y, Wu M, Sham JST, Tai L, Fang Y, Wu W, et al. Different expression of hepatitis B surface antigen between hepatocellular carcinoma and its surrounding liver tissue, studied using a tissue microarray. J Pathology. 2002;197:610–6.

11. Tantiwetrueangdet A, Panvichian R, Sornmayura P, Sueangoen N, Leelaudomlipi S. Reduced HBV cccDNA and HBsAg in HBV-associated hepatocellular carcinoma tissues. Méd Oncol (Northwood, Lond, Engl). 2018;35:127.

12. Fu S, Li N, Zhou PC, Huang Y, Zhou R rong, Fan XG. Detection of HBV DNA and antigens in HBsAg-positive patients with primary hepatocellular carcinoma. Clin Res Hepatol Gas. 2017;41:415–23.

13. Tan AT, Yang N, Krishnamoorthy TL, Oei V, Chua A, Zhao X, et al. Use of Expression Profiles of HBV-DNA Integrated Into Genomes of Hepatocellular Carcinoma Cells to Select T Cells for Immunotherapy. Gastroenterology. 2019;156:1862-1876.e9.

14. Srivastava M, Copin R, Choy A, Zhou A, Olsen O, Wolf S, et al. Proteogenomic identification of Hepatitis B virus (HBV) genotype-specific HLA-I restricted peptides from HBV-positive patient liver tissues. Front Immunol. 2022;13:1032716.

15. Beijer MTA de, Bezstarosti K, Luijten R, Doff WAS, Boor PPC, Pieterman RFA, et al. Immunopeptidome of hepatocytes isolated from patients with HBV infection and hepatocellular carcinoma. JHEP Rep. 2022;4:100576.

16. Gehring AJ, Xue SA, Ho ZZ, Teoh D, Ruedl C, Chia A, et al. Engineering virus-specific T cells that target HBV infected hepatocytes and hepatocellular carcinoma cell lines. J Hepatol. 2011;55:103–10.

17. Wisskirchen K, Metzger K, Schreiber S, Asen T, Weigand L, Dargel C, et al. Isolation and functional characterization of hepatitis B virus-specific T-cell receptors as new tools for experimental and clinical use. Plos One. 2017;12:e0182936.

18. Wisskirchen K, Kah J, Malo A, Asen T, Volz T, Allweiss L, et al. T cell receptor grafting allows virological control of Hepatitis B virus infection. J Clin Invest. 2019;129:2932–45.

19. Sommermeyer D, Uckert W. Minimal Amino Acid Exchange in Human TCR Constant Regions Fosters Improved Function of TCR Gene-Modified T Cells. J Immunol. 2010;184:6223–31.

20. Porter DL, Hwang WT, Frey NV, Lacey SF, Shaw PA, Loren AW, et al. Chimeric antigen receptor T cells persist and induce sustained remissions in relapsed refractory chronic lymphocytic leukemia. Sci Transl Med. 2015;7:303ra139.

21. Louis CU, Savoldo B, Dotti G, Pule M, Yvon E, Myers GD, et al. Antitumor activity and long-term fate of chimeric antigen receptor–positive T cells in patients with neuroblastoma. Blood. 2011;118:6050–6.

22. Festag J, Festag M, Asen T, Wettengel J, Mück-Häusl M, Abdulhaqq S, et al. Vector-mediated delivery of human MHC-I into hepatocytes enables investigation of TCR-redirected HBV-specific T cells in mice and macaque cell cultures. Hum Gene Ther. 2023;0.

23. Lee DW, Santomasso BD, Locke FL, Ghobadi A, Turtle CJ, Brudno JN, et al. ASTCT Consensus Grading for Cytokine Release Syndrome and Neurologic Toxicity Associated with Immune Effector Cells. Biol Blood Marrow Tr. 2019;25:625–38.

24. Shimabukuro-Vornhagen A, Gödel P, Subklewe M, Stemmler HJ, Schlößer HA, Schlaak M, et al. Cytokine release syndrome. J Immunother Cancer. 2018;6:56.

25. Turtle CJ, Hanafi LA, Berger C, Gooley TA, Cherian S, Hudecek M, et al. CD19 CAR–T cells of defined CD4+:CD8+ composition in adult B cell ALL patients. J Clin Invest. 2016;126:2123–38.

26. Muranski P, Boni A, Wrzesinski C, Citrin DE, Rosenberg SA, Childs R, et al. Increased intensity lymphodepletion and adoptive immunotherapy—how far can we go? Nat Clin Pract Oncol. 2006;3:668–81.

27. Kielsen K, Oostenbrink LVE, Asmuth EGJ von, Jansen-Hoogendijk AM, Dam MM van O ten, Ifversen M, et al. IL-7 and IL-15 Levels Reflect the Degree of T Cell Depletion during Lymphopenia and Are Associated with an Expansion of Effector Memory T Cells after Pediatric Hematopoietic Stem Cell Transplantation. J Immunol. 2021;206:2828–38.

28. Heczey A, Louis CU, Savoldo B, Dakhova O, Durett A, Grilley B, et al. CAR T Cells Administered in Combination with Lymphodepletion and PD-1 Inhibition to Patients with Neuroblastoma. Mol Ther. 2017;25:2214–24.

29. Festag MM, Festag J, Fräßle SP, Asen T, Sacherl J, Schreiber S, et al. Evaluation of a Fully Human, Hepatitis B Virus-Specific Chimeric Antigen Receptor in an Immunocompetent Mouse Model. Mol Ther. 2019;27:947–59.

30. Lampertico P, Agarwal K, Berg T, Buti M, Janssen HLA, Papatheodoridis G, et al. EASL 2017 Clinical Practice Guidelines on the management of hepatitis B virus infection. J Hepatol. 2017;67:370–98.

31. Shouval D. Adoptive transfer of immunity to HBV in liver transplant patients:A step forward toward the proof of concept for therapeutic vaccination or a transient immunologic phenomenon? Liver Transplant. 2007;13:14–7.

32. Sonneveld MJ, Zoutendijk R, Flink HJ, Zwang L, Hansen BE, Janssen HLA. Close Monitoring of Hepatitis B Surface Antigen Levels Helps Classify Flares During Peginterferon Therapy and Predicts Treatment Response. Clin Infect Dis Official Publ Infect Dis Soc Am. 2013;56:100–5.

33. Chi H, Arends P, Reijnders JGP, Carey I, Brown A, Fasano M, et al. Flares during long-term entecavir therapy in chronic hepatitis B. J Gastroenterol Hepatol. 2016;31:1882–7.

34. Montanari NR, Ramírez R, Aggarwal A, Buuren N van, Doukas M, Moon C, et al. Multi-parametric analysis of human livers reveals variation in intrahepatic inflammation across phases of chronic hepatitis B infection. J Hepatol. 2022;77:332–43.

35. Meier MA, Calabrese D, Suslov A, Terracciano LM, Heim MH, Wieland S. Ubiquitous expression of HBsAg from integrated HBV DNA in patients with low viral load. J Hepatol. 2021;75:840–7.

36. Aggarwal A, Odorizzi PM, Brodbeck J, Buuren N van, Moon C, Chang S, et al. Intrahepatic quantification of HBV antigens in chronic hepatitis B reveals heterogeneity and treatment-mediated reductions in HBV core-positive cells. Jhep Reports. 2023;5:100664.

37. Cheng PN, Chiu YC, Tsai HW, Wang RH, Chiu HC, Wu IC, et al. HBsAg expression of liver correlates with histological activities and viral replication in chronic hepatitis B. Ann Hepatol. 2014;13:771–80.

38. Chu CM, Liaw YF. Membrane staining for hepatitis B surface antigen on hepatocytes: a sensitive and specific marker of active viral replication in hepatitis B. J Clin Pathol. 1995;48:470.

39. Wursthorn K, Lutgehetmann M, Dandri M, Volz T, Buggisch P, Zollner B, et al. Peginterferon alpha-2b plus adefovir induce strong cccDNA decline and HBsAg reduction in patients with chronic hepatitis B. Hepatology. 2006;44:675–84.

40. Thompson AJV, Nguyen T, Iser D, Ayres A, Jackson K, Littlejohn M, et al. Serum hepatitis B surface antigen and hepatitis B e antigen titers: Disease phase influences correlation with viral load and intrahepatic hepatitis B virus markers. Hepatology. 2010;51:1933–44.

41. Chen W, Zhang K, Dong P, Fanning G, Tao C, Zhang H, et al. Noninvasive chimeric DNA profiling identifies tumor-originated HBV integrants contributing to viral antigen expression in liver cancer. Hepatol Int. 2020;14:326–37.

42. Svicher V, Salpini R, Piermatteo L, Carioti L, Battisti A, Colagrossi L, et al. Whole exome HBV DNA integration is independent of the intrahepatic HBV reservoir in HBeAg-negative chronic hepatitis B. Gut. 2021;70:2337–48.

43. Rydell GE, Larsson SB, Prakash K, Andersson M, Norder H, Hellstrand K, et al. Abundance of non-circular intrahepatic hepatitis B virus DNA may reflect frequent integration into human DNA in chronically infected patients. J Infect Dis. 2020;225:572-.

44. Grudda T, Hwang HS, Taddese M, Quinn J, Sulkowski MS, Sterling RK, et al. Integrated hepatitis B virus DNA maintains surface antigen production during antivirals. J Clin Invest. 2022;132:e161818.

45. Revill P, Testoni B, Locarnini S, Zoulim F. Global strategies are required to cure and eliminate HBV infection. Nat Rev Gastroentero. 2016;13:239–48.

46. Yuen M, Schiefke I, Yoon J, Ahn SH, Heo J, Kim JH, et al. RNA Interference Therapy With ARC-520 Results in Prolonged Hepatitis B Surface Antigen Response in Patients With Chronic Hepatitis B Infection. Hepatology. 2020;72:19–31.

47. Wooddell CI, Yuen MF, Chan HLY, Gish RG, Locarnini SA, Chavez D, et al. RNAi-based treatment of chronically infected patients and chimpanzees reveals that integrated hepatitis B virus DNA is a source of HBsAg. Sci Transl Med. 2017;9.

48. Wooddell CI, Gehring AJ, Yuen MF, Given BD. RNA Interference Therapy for Chronic Hepatitis B Predicts the Importance of Addressing Viral Integration When Developing Novel Cure Strategies. Viruses. 2021;13:581.

49. Cornberg M, Manns MP. No cure for hepatitis B and D without targeting integrated viral DNA? Nat Rev Gastroentero. 2018;15:195–6.

50. Nagarsheth NB, Norberg SM, Sinkoe AL, Adhikary S, Meyer TJ, Lack JB, et al. TCR-engineered T cells targeting E7 for patients with metastatic HPV-associated epithelial cancers. Nat Med. 2021;1–7.

51. Baudi I, Kawashima K, Isogawa M. HBV-Specific CD8+ T-Cell Tolerance in the Liver. Front Immunol. 2021;12:721975.

52. You M, Gao Y, Fu J, Xie R, Zhu Z, Hong Z, et al. Epigenetic regulation of HBV-specific tumor-infiltrating T cells in HBV-related HCC. Hepatology. 2023;78:943–58.

53. Meng F, Zhao J, Tan AT, Hu W, Wang SY, Jin J, et al. Immunotherapy of HBV-related advanced hepatocellular carcinoma with short-term HBV-specific TCR expressed T cells: results of dose escalation, phase I trial. Hepatol Int. 2021;15:1402–12.

54. Tan AT, Meng F, Jin J, Zhang J, Wang S, Shi L, et al. Immunological alterations after immunotherapy with short lived HBV-TCR T cells associates with long-term treatment response in HBV-HCC. Hepatol Commun. 2022;6:841–54.

55. Silver HK, Deneault J, Gold P, Thompson WG, Shuster J, Freedman SO. The detection of alpha 1-fetoprotein in patients with viral hepatitis. Cancer Res. 1974;34:244–7.

56. Hanif H, Ali MJ, Susheela AT, Khan IW, Luna-Cuadros MA, Khan MM, et al. Update on the applications and limitations of alpha-fetoprotein for hepatocellular carcinoma. World J Gastroenterol. 2022;28:216–29.

57. Qasim W, Brunetto M, Gehring AJ, Xue SA, Schurich A, Khakpoor A, et al. Immunotherapy of HCC metastases with autologous T cell receptor redirected T cells, targeting HBsAg in a liver transplant patient. J Hepatol. 2015;62:486–91.

58. Sommermeyer D, Hudecek M, Kosasih PL, Gogishvili T, Maloney DG, Turtle CJ, et al. Chimeric antigen receptor-modified T cells derived from defined CD8+ and CD4+ subsets confer superior antitumor reactivity in vivo. Leukemia. 2016;30:492–500.

59. Li Y, Wu D, Yang X, Zhou S. Immunotherapeutic Potential of T Memory Stem Cells. Front Oncol. 2021;11:723888.

60. Biasco L, Izotova N, Rivat C, Ghorashian S, Richardson R, Guvenel A, et al. Clonal expansion of T memory stem cells determines early anti-leukemic responses and long-term CAR T cell persistence in patients. Nat Cancer. 2021;2:629–42.

61. Reinhard K, Rengstl B, Oehm P, Michel K, Billmeier A, Hayduk N, et al. An RNA vaccine drives expansion and efficacy of claudin-CAR-T cells against solid tumors. Science. 2020;367:446–53.

Figure 1. Properties of the clinical HBV-specific T cell product SCG101.

(A) Schematic structure of the HLA-A*02-restricted, HBV S20-specific T cell receptor (TCR) SCG101 used for transduction of T cells. To increase TCR expression and correct pairing, TCR chains were codon-optimized, and an additional cysteine bond (orange, dashed line) was introduced to the constant domains. The human constants harbored nine amino acids from the murine TCR constant domains as indicated (red lines). (**B)** Binding strengths of TCR SCG101 expressed in Jurkat cells. Jurkat-SCG101 were stained with decreasing amounts of HLA-A*02:01-S20 (FLLTRILTI)-PE-labeled multimers (blue circles) or with an HLA-A*02:01-C18 (FLPSDFFPSV) multimer (red circles) as negative control. The mean fluorescence intensity (MFI) was quantified by flow cytometry. (**C)** TCR expression in $CD8^+$ and $CD4^+$ T cells after lentiviral transduction. The binding of a PE-labeled S20-multimer indicates correctly paired TCR chains and Vβ5.1-FITC staining indicates the proportion of transduced T cells. Quantification of the potential TCR mispairing rate in % as a quotient of total multimer+ cells divided by (total Vβ5.1+ cells – endogenously expressing Vβ5.1+ cells). Mean +/- SEM for six batches of SCG101-T is shown. Untransduced cells (UT) served as a control to quantify T cells endogenously expressing Vβ5.1. **(D)** Estimation of the SCG101 recognition motif by alanine scanning. Each native residue of peptide S20 (FLLTRILTI) was substituted at each position for an alanine. T2 cells were pulsed with 1 µM of each modified peptide indicated on the x-axis and co-cultured with SCG101 TCR-T, the IFN-γ concentration was measured by CBA. The prototype S20-gtA/D and the C18 peptide were set as positive or negative controls, respectively. **(E)** Cross-reactivity screening of SCG101 against human peptides containing the core binding motif L3 / T4 / R5 / I6 at concentrations of 1 (blue circles) and 0.1 (red circles) µg/ml. **(F)** Cross-reactivity of SCG101 against human peptides containing ≥ six amino acid sites consistent with the S20 peptide. S20 peptide FLLTKILTI represents a variant often found in HBV genotypes B and C. Mean values of duplicates are shown. The labeling indicates the name of the human gene containing the respective peptide sequence.

Figure 1

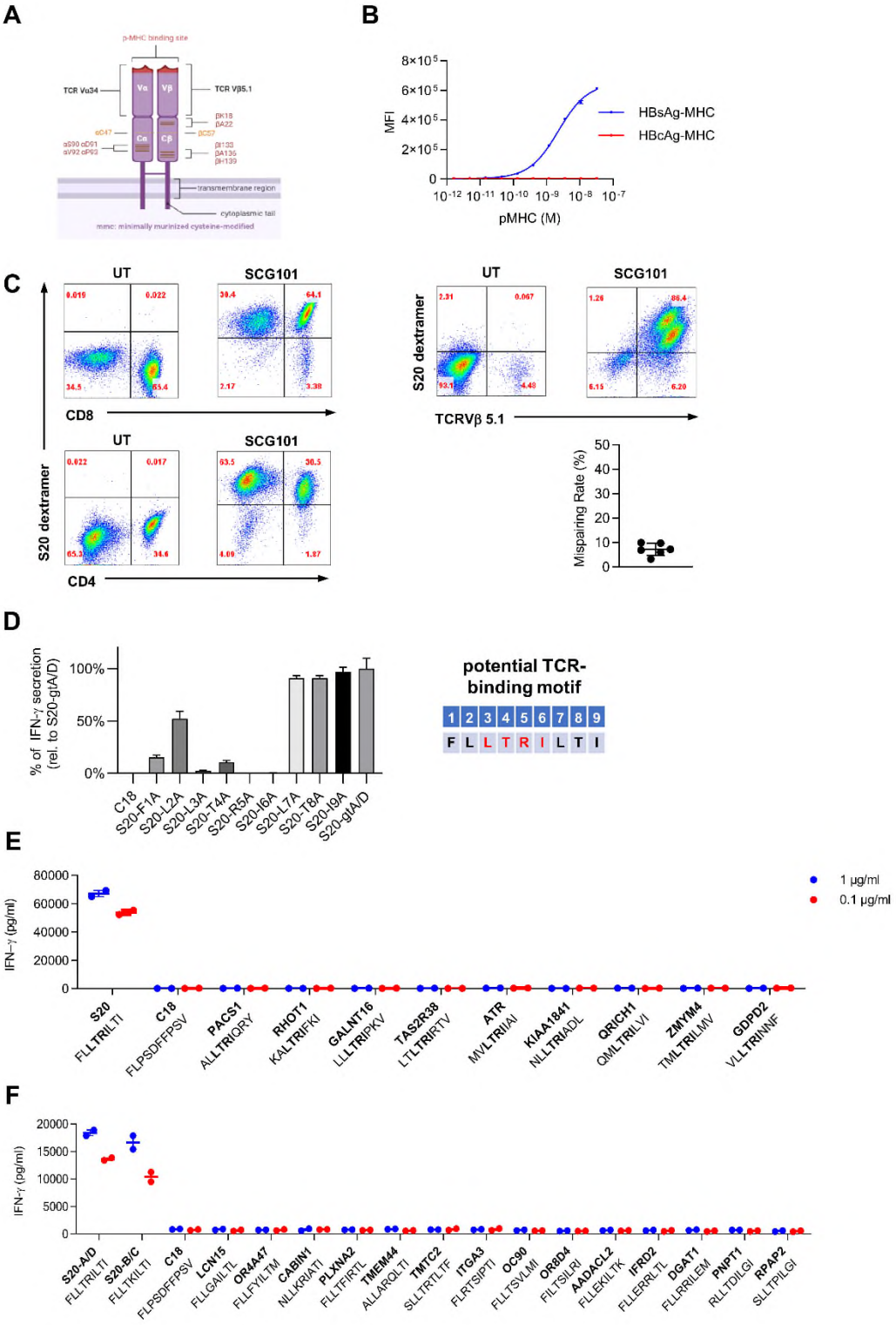
A
p-MHC binding site
TCR Vα34
TCR Vβ5.1
Vα
Vβ
Cα
Cβ
αC47
αG90 αD91
αV92 αP93
βK18
βA22
βC57
βI133
βA135
βK139
transmembrane region
cytoplasmic tail
mmc: minimally murinized cysteine-modified
B
MFI
HBsAg-MHC
HBcAg-MHC
pMHC (M)
C
UT
SCG101
CD8
CD4
S20 dextramer
TCRVβ 5.1
Mispairing Rate (%)
D
% of IFN-γ secretion (rel. to S20-gtA/D)
C18
S20-F1A
S20-L2A
S20-L3A
S20-T4A
S20-R5A
S20-I6A
S20-L7A
S20-T8A
S20-I9A
S20-gtA/D
potential TCR-binding motif
1 2 3 4 5 6 7 8 9
F L L T R I L T I
E
IFN-γ (pg/ml)
1 µg/ml
0.1 µg/ml
S20 FLLTRILTI
C18 FLPSDFFPSV
PACS1 ALLTRIQRY
RHOT1 KALTRIFKI
GALNT16 LLLTRIPKV
TAS2R38 LTLTRIRTV
ATR MVLTRIIAI
KIAA1841 NLLTRIADL
QRICH1 QMLTRILVI
ZMYM4 TMLTRILMV
GDPD2 VLLTRINNF
F
IFN-γ (pg/ml)
S20-A/D FLLTRILTI
S20-B/C FLLTKILTI
C18 FLPSDFFPSV
LCN15 FLLGAILTL
OR4A47 FLLFYILTM
CABIN1 NLLKRIATI
PLXNA2 FLLTFIRTL
TMEM44 ALLARQLTI
TMTC2 SLLTRTLTF
ITGA3 FLRTSIPTI
OC90 FLLTSVLMI
OR8D4 FILTSILRI
AADACL2 FLLEKILTK
IFRD2 FLLERRLTL
DGAT1 FLLRRILEM
PNPT1 RLLTDILGI
RPAP2 SLLTPILGI

761

762 **Figure 2. *In vitro* potency of the HBV-specific T-cell product SCG101.**

763 **(A)** The functional avidity of SCG101 T cells was assessed by titration of the S20 peptide (blue
764 circles) loaded on T2 cells. The concentration of IFN-γ, TNF-α, and IL-2 in supernatants after
765 24 hours of co-culture was measured by Cytokine Bead Array (CBA). C18 peptide (red circles)
766 loading served as a negative control. **(B)** Cytolysis of tumor cell lines determined by the
767 impedance of adherent target cells via xCELLigence real-time measurement. HBsAg negative
768 (left) or positive (right) HepG2 target cells were co-cultured with SCG101 (blue lines) or
769 untransduced (UT, red lines) at an effector-to-target (E:T) ratio of 1:1 (solid lines) or 1:5 (dashed
770 lines). Mean values are shown. **(C)** Supernatants of the co-cultures were analyzed for IFN-γ
771 after 48 hours by CBA. **(D)** HBsAg in supernatants after 48 hours of co-culture was measured
772 by a quantitative ELISA. Data from two donors (C,D mean +/- SEM) are shown.

Figure 2

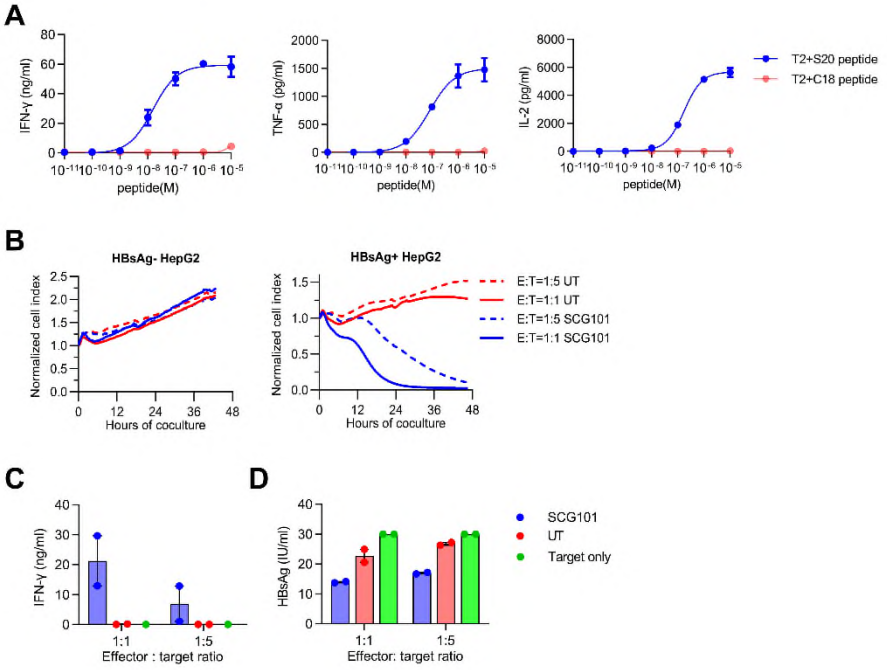
A
IFN-γ (ng/ml)
peptide(M)
TNF-α (pg/ml)
peptide(M)
IL-2 (pg/ml)
peptide(M)
T2+S20 peptide
T2+C18 peptide
B
HBsAg- HepG2
HBsAg+ HepG2
Normalized cell index
Hours of coculture
E:T=1:5 UT
E:T=1:1 UT
E:T=1:5 SCG101
E:T=1:1 SCG101
C
IFN-γ (ng/ml)
Effector : target ratio
D
HBsAg (IU/ml)
Effector: target ratio
SCG101
UT
Target only

774 **Figure 3. *In vivo* anti-tumor potency of HBV-specific SCG101 T cells.**

775 **(A)** NOD-Cg-PrkdcSCIDIL-2Rgcnull/vst (NPG) mice (female:male=1:1) were subcutaneously
776 inocu-lated with 1×10^7 HBsAg+ hepatoma cells/animal in the right armpit. After six days, 60
777 animals were divided into six groups. Mice received either increasing numbers of SCG101,
778 multimer positive T cells of 0.2 to 2×10^7 TCR-T cells/animal, or a mixture of CS10, HSA, and
779 sodium chloride (vehicle, black lines), or untransduced T cells (UT, 4.3×10^7 cells/animal, brown
780 lines) according to the total number of T cells in the highest SCG101 group. Injections were
781 done intravenously and **(B)** body weight and **(C)** tumor volume were analyzed twice weekly.
782 Mean +/- SEM of n=10 per group, 5 male (circles), 5 female (squares) are shown, *** =
783 $P\leq0.001$.

Figure 3

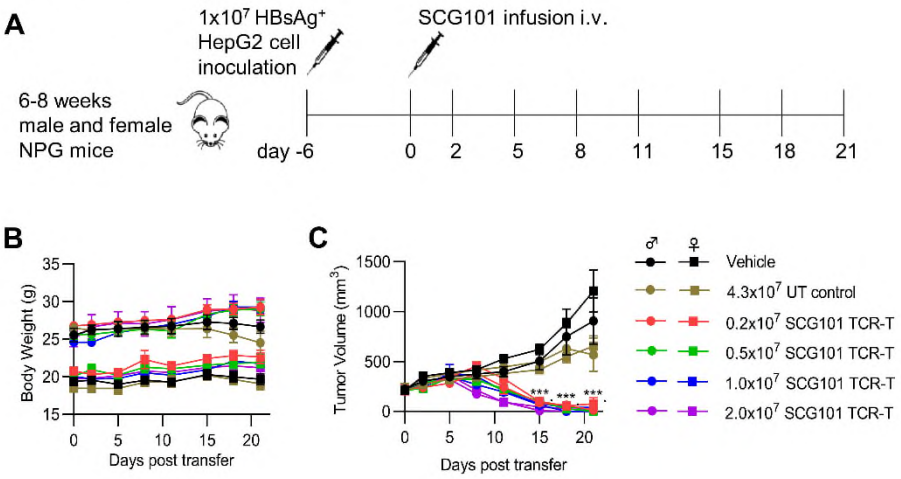
A
1x10^7 HBsAg+
HepG2 cell
inoculation
SCG101 infusion i.v.
6-8 weeks
male and female
NPG mice
day -6
0
2
5
8
11
15
18
21
B
Body Weight (g)
Days post transfer
C
Tumor Volume (mm^3)
Days post transfer
♂
♀
Vehicle
4.3x10^7 UT control
0.2x10^7 SCG101 TCR-T
0.5x10^7 SCG101 TCR-T
1.0x10^7 SCG101 TCR-T
2.0x10^7 SCG101 TCR-T

Figure 4. Patient characteristics. (A) Scheme of the medical history of HCC diagnosis and treatment of patient ST1206. Study enrollment was initiated after the failure of three prior HCC treatments (resection, transarterial chemoembolization (TACE) with Raltitrexed and Lobaplatin, and Sorafenib). **(B)** HLA profile and status of liver disease of patient ST1206 including Child-Pugh-Score, Eastern Co-operative Oncology Group (ECOG) performance status, Barcelona clinic liver cancer (BCLC) staging, and China liver cancer (CNLC) classification. Blue lines indicate duration of systemic treatments. ETV= Entecavir **(C-F)** Immunohistological analysis of a liver biopsy taken three months prior to treatment. Four pieces of non-tumor liver tissue were obtained, and representative sections are shown. Scale bars: 200 µm and 40 µm (inlay), respectively. The circle indicates the orientation of the inlay. **(C)** Morphological analysis using hematoxylin and eosin (H&E) staining. Immunostainings for **(D)** HLA-A, **(E)** HBcAg, and **(F)** HBsAg (three different sections are shown because of a diverse expression profile)

Figure 4

A

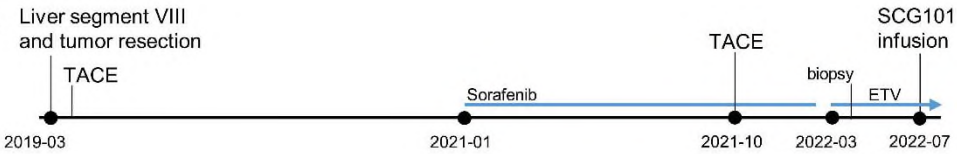

B

Age	Gender	HLA-A	HLA-B	HLA-C	Child-P. score	ECOG status	BCLC stage	CNLC stage
54	male	*02:01 *23:01	*39:24 *44:03	*04:01 *07:01	A	0	B	IIb

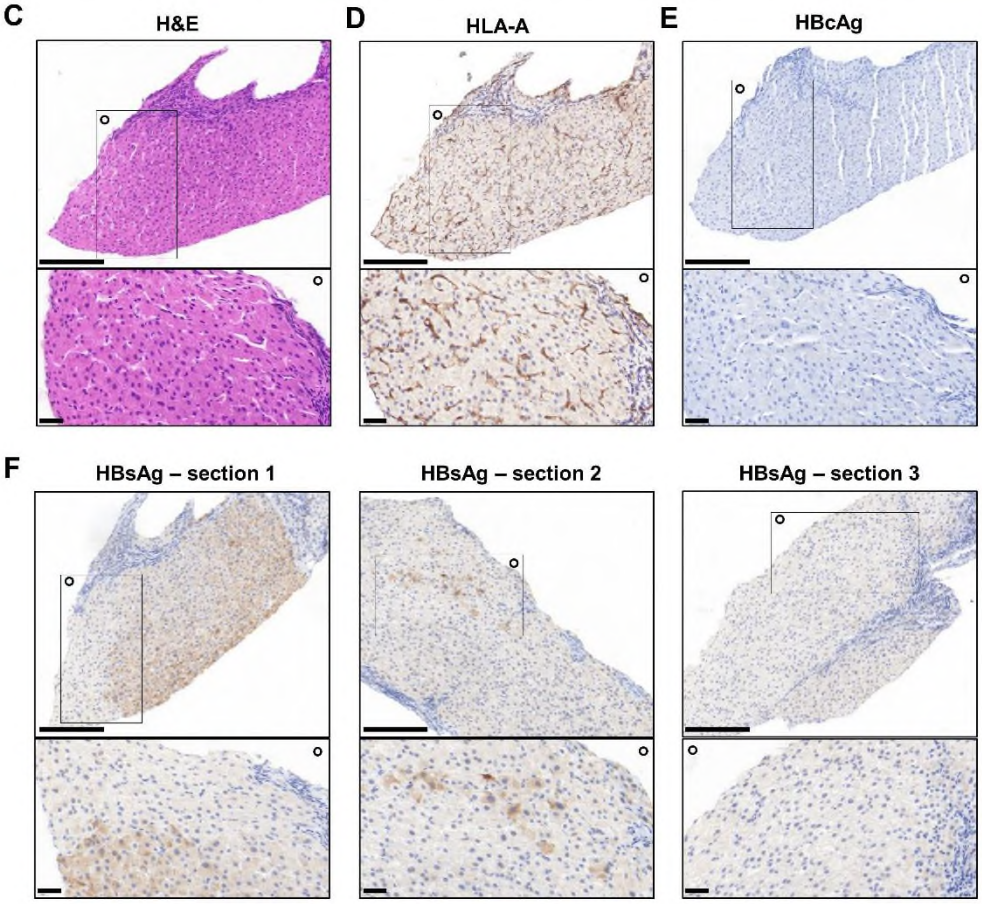

Figure 5. Liver and cytokine serum markers after transfer of SCG101 HBV-specific T cells. (A) Scheme of the drug administration (black circles) and tumor assessments (white circles). Following Cy/Flu lymphodepletion on days -6 to -4, a single dose of $7.9x10^7$/kg (5.9×10^9 total) TCR-T cells was infused intravenously. Red lines indicate blood sample collections. **(B-H)** Serum markers of liver function, alanine transaminase (ALT), aspartate transaminase (AST), LDH, TBIL (total bilirubin), ferritin, albumin, and the INR were measured on indicated days. A grey area indicates the normal range. **(I)** C-reactive protein (CRP) indicating ongoing inflammation. **(J-M)** Serum concentrations of IL-6, IFN-γ, IL-2, and IL-10 were determined by CBA. LOD: limit of detection, LD: lymphodepletion, ACT: adoptive cell transfer.

Figure 5

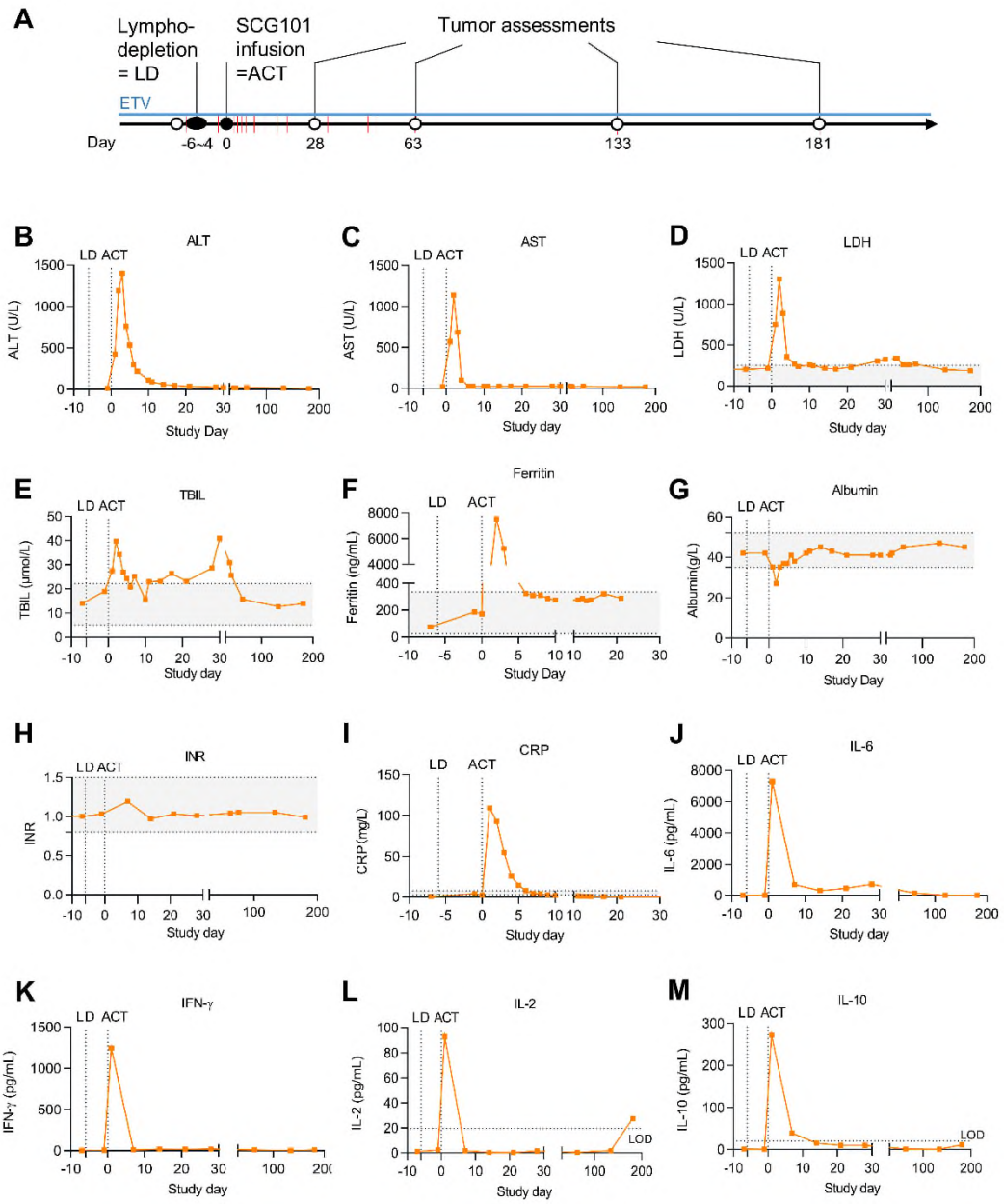
A
Lympho-
depletion
= LD
SCG101
infusion
=ACT
Tumor assessments
ETV
Day
-6~4
0
28
63
133
181
B
ALT
LD ACT
ALT (U/L)
Study Day
C
AST
LD ACT
AST (U/L)
Study day
D
LDH
LD ACT
LDH (U/L)
Study day
E
TBIL
LD ACT
TBIL (μmol/L)
Study day
F
Ferritin
LD
ACT
Ferritin (ng/mL)
Study Day
G
Albumin
LD ACT
Albumin(g/L)
Study Day
H
INR
LD ACT
INR
Study day
I
CRP
LD
ACT
CRP (mg/L)
Study day
J
IL-6
LD ACT
IL-6 (pg/mL)
Study day
K
IFN-γ
LD ACT
IFN-γ (pg/mL)
Study day
L
IL-2
LD ACT
IL-2 (pg/mL)
LOD
Study day
M
IL-10
LD ACT
IL-10 (pg/mL)
LOD
Study day

Figure 6. *Ex vivo* analysis of transferred T cells. (A) Flow cytometry gating strategy exemplified with a blood sample taken 21 days post transfer. Single living lymphocytes were gated first and followed by identification of transferred cells via anti-CD3 and HBV S20-dextramer staining. In two separate staining panels, dextramer binding TCR+ T cells were stained either for the T cell subsets with anti-CD8 and anti-CD4, or for memory differentiation status with anti-CCR7 and anti-CD45RA. Given the unspecific stimulation during T cell transduction and the antigen encounter after infusion, $CCR7^+$ $CD45RA^+$ cells were considered T_{SCM} and not naïve cells. The FMO (fluorescence minus one) control shows a staining without dextramer. **(B, C)** Flow cytometry analysis of blood samples taken after the cell transfer, gated on $CD3^+$ and HBV-S20-dextramer$^+$ cells (blue circles). TCR^+ T cells stained either for the T-cell subsets with anti-CD8 (pink triangle) or anti-CD4 (purple triangle), or for memory differentiation status with anti-CCR7 and anti-CD45RA. T_{CM}:$CCR7^+CD45RA^-$ (red squares), T_{SCM}:$CCR7^+CD45RA^+$ (green triangle), T_{EM}:$CCR7^-CD45RA^-$ (black circles), T_{EFF}:$CCR7^-$ $CD45RA^+$ (orange diamond). Different T-cell phenotypes were analyzed on indicated days and quantified using counting beads. **(D)** Genomic DNA was extracted from blood samples and the viral copy number (VCN) was quantified via qPCR.

Figure 6

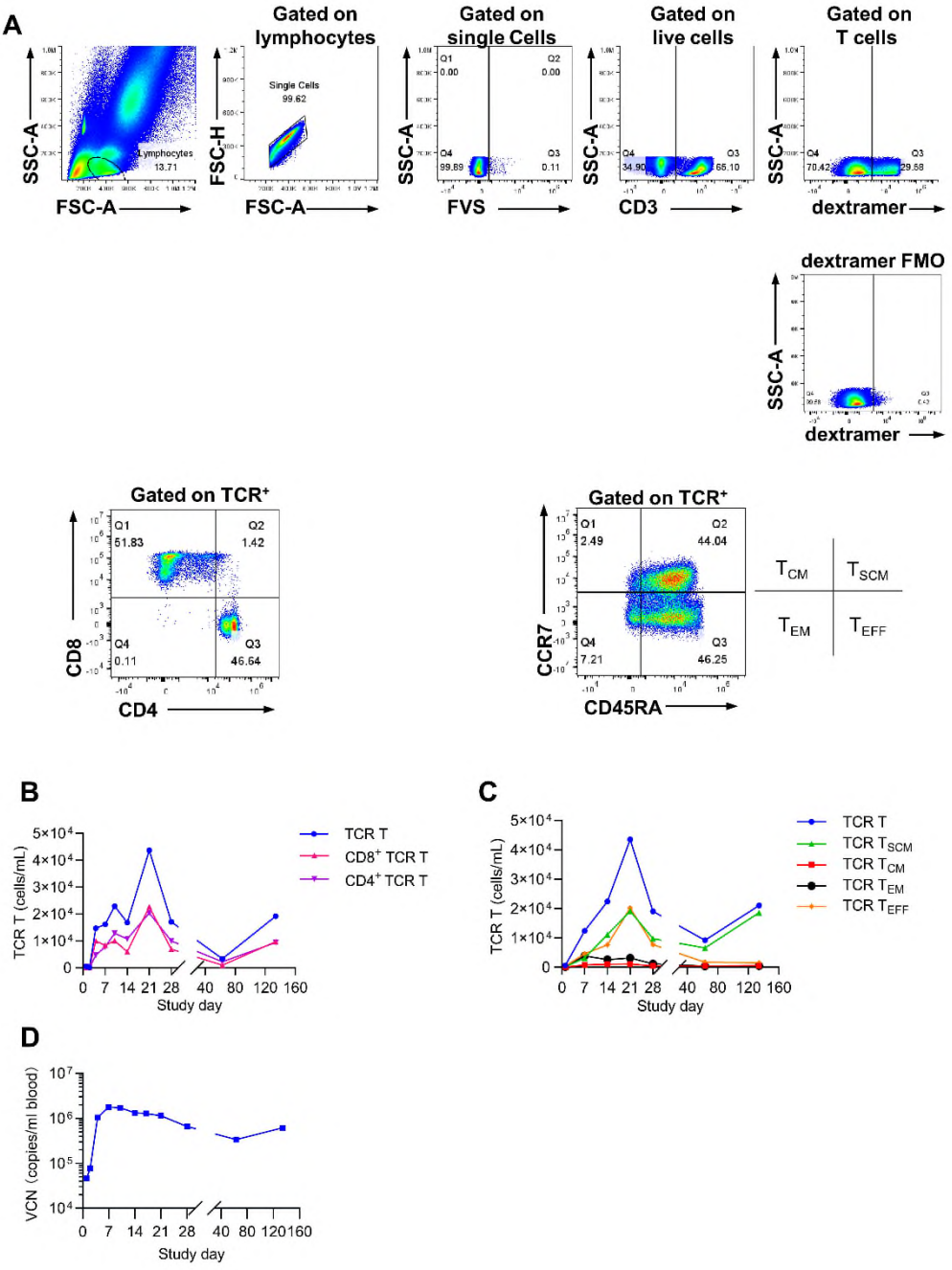
A
Gated on lymphocytes
Gated on single Cells
Gated on live cells
Gated on T cells
SSC-A
FSC-A
Lymphocytes
13.71
FSC-H
Single Cells
99.62
FVS
CD3
dextramer
dextramer FMO
Gated on TCR+
CD8
CD4
Q1
51.83
Q2
1.42
Q4
0.11
Q3
46.64
CCR7
CD45RA
Q1
2.49
Q2
44.04
Q4
7.21
Q3
46.25
TCM
TSCM
TEM
TEFF
B
TCR T (cells/mL)
Study day
TCR T
CD8+ TCR T
CD4+ TCR T
C
TCR T
TCR TSCM
TCR TCM
TCR TEM
TCR TEFF
D
VCN (copies/ml blood)
Study day

Figure 7. Antiviral and antitumor response after treatment with HBV-specific SCG101 T cells.

(A) HBsAg (left axis, blue squares) was measured in serum at indicated time points. The diagnostic ELISA´s lower limit of detection (LoD) was 0.05 IU/ml. ALT values (right axis, orange line) from Figure 6B were plotted again to better visually correlate both markers. The adoptive cell transfer (ACT) time point is indicated with a dashed line. **(B)** HBV-DNA was measured in sera via qPCR. **(C)** Immunostaining of HBsAg of a liver biopsy taken 73 days after treatment. One piece of non-tumor liver tissue was obtained. Scale bars: 200 µm and 50 µm (inlay), respectively. **(D)** The tumor burden was analyzed via multiphasic CT scan on days -7 prior to treatment and on days 28, 63, 133, and 181 after ACT. The size of the target (T) lesion no.1 and no.2 in mRECIST (m) or iRECIST (i) and the position of non-target (NT) lesions are indicated in yellow.

Figure 7

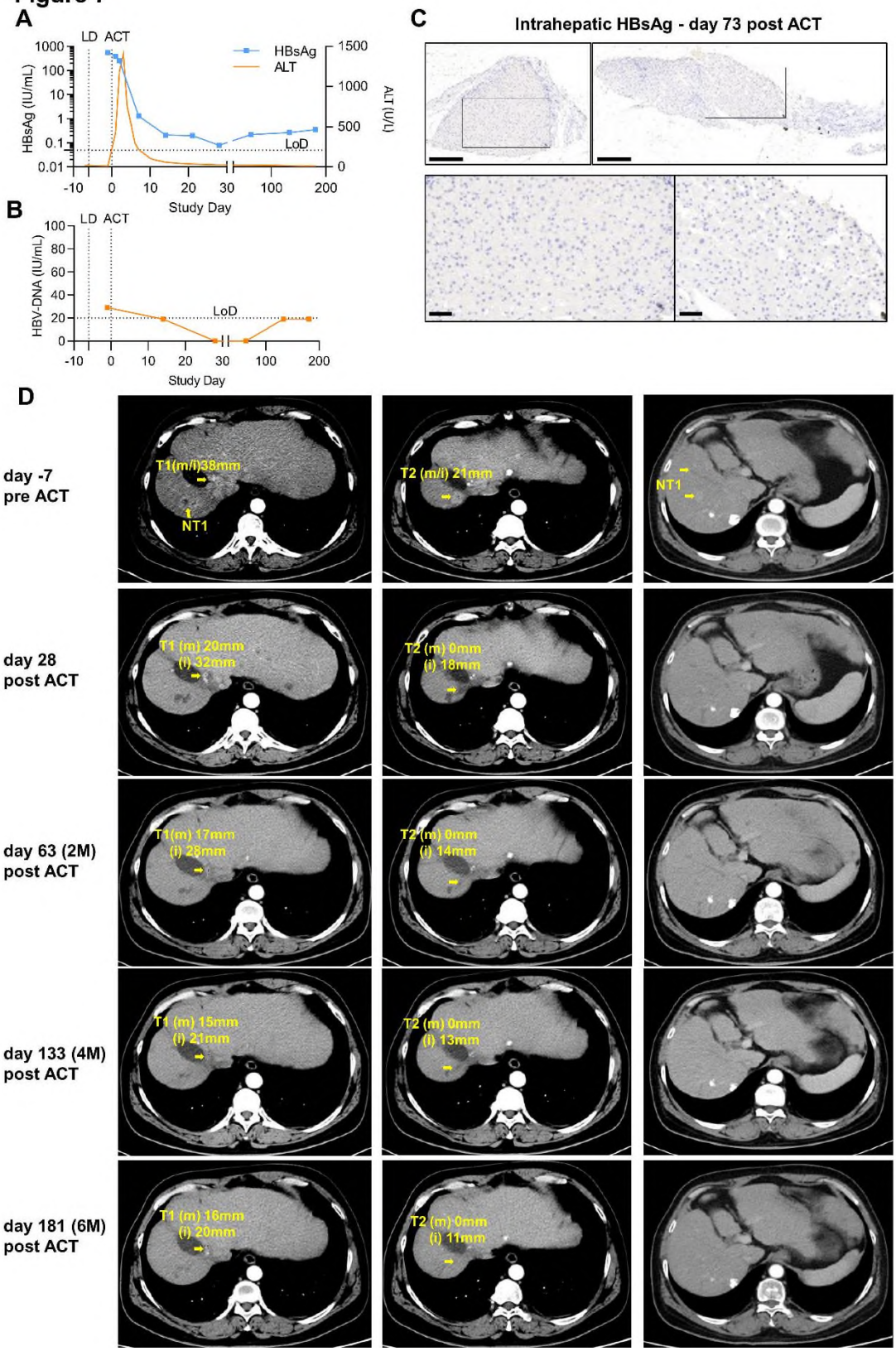
A
LD ACT
HBsAg
ALT
HBsAg (IU/mL)
ALT (U/L)
LoD
Study Day
B
LD ACT
HBV-DNA (IU/mL)
LoD
Study Day
C
Intrahepatic HBsAg - day 73 post ACT
D
day -7
pre ACT
T1(m/i)38mm
NT1
T2 (m/i) 21mm
NT1
day 28
post ACT
T1 (m) 20mm
(i) 32mm
T2 (m) 0mm
(i) 18mm
day 63 (2M)
post ACT
T1(m) 17mm
(i) 28mm
T2 (m) 0mm
(i) 14mm
day 133 (4M)
post ACT
T1 (m) 15mm
(i) 21mm
T2 (m) 0mm
(i) 13mm
day 181 (6M)
post ACT
T1 (m) 16mm
(i) 20mm
T2 (m) 0mm
(i) 11mm

Table 1. Treatment-related adverse events ≥grade 3

TRAE	Highest Severity	Relation with SCG101	Other possible reasons	≥G3 AE duration
CRS	Grade 3	Definitely related	\	G3: D1-3
Hypotension	Grade 3	Possibly related	\	G3: D1-2
Decreased white cell count	Grade 4	Possibly related	Lymphodepletion	G4: D0-4 G3: D4-5, D14-17, D21-22, D28-30, 31-34
Decreased neutrophil count	Grade 4	Possibly related	Lymphodepletion	G4: D2-4, D28-30 G3: D0-2, 13-17, 31-34, 48-52
Decreased platelet count	Grade 4	Possibly related	Lymphodepletion	G4: D2-3, D4-6, D21-28 G3: D0-2, D3-4, D6-11, D12-13, D14-21
	Grade 3	Possibly related	Hepatocellular carcinoma	G3: D30-43, D77-80
Decreased lymphocyte count	Grade 3	Possibly related	Lymphodepletion	G3: D28-31
Increased ALT	Grade 4	Possibly related	Lymphodepletion	G4: D2-4 G3: D1-2, D4-7
Increased AST	Grade 4	Possibly related	Lymphodepletion	G4: D2-3 G3: D1-2, D3-4

Note: All these ⩾grade 3 were resolved or returned to baseline at the end of the AE.

(TRAE: treatment related adverse event, G3: grade 3, G4: grade 4)

Supplementary Methods

TCR lentiviral constructs

The TCR nucleotide sequence of SCG101 was isolated from a donor with resolved HBV infection.[1] It was codon-optimized for expression in human tissues, synthesized, and cloned into the pCDH lentivirus backbone with a P2A linker to connect the TCR Vα34 and Vβ5.1 chain. Besides codon-optimization and an additional cysteine bond between the constant domains, nine amino acids of the human constant domains were murinized [2] to increase correct TCR pairing and yet keep xenogeneic sequences and potential immunogenicity at a minimum (mmc=minimally murinized, cysteine-modified). The TCR was not subject to further artificial affinity enhancement or maturation.

Flow cytometry

Cells were labeled with antibodies against CD3, CD4, CD8, CD45RA, CCR7 (BD Biosciences), and TCRvβ5.1 (Miltenyi Biotec) at the recommended dilution in PBS with 2% FBS. Staining for correctly paired TCRs was performed with S20-HLA-A*02:01 dextramer (WB3290, Immudex) simultaneously with the antibody staining. The Fixable Viability Stain (FVS) 780 (BD Biosciences) was used for live/dead staining.

To measure the TCR binding strength, TCR-expressing Jurkat cells were incubated with serially diluted ($3.2x10^{-8}$ to $1.6x10^{-12}$ M) PE-labelled dextramers. A PE-labelled HBcAg C18 dextramer (FLPSDFFPSV, Immudex WB3289-PE) served as a control.

Data were acquired on a CytoFLEX flow cytometer (Beckman Coulter) and analyzed with FlowJo software version V10 (BD).

Mismatch peptide testing

The potential TCR binding motif, as determined by alanine-scan, focused on key amino acid positions (3/4/5/6) and provided a basis for computer-based predictive analysis to assess the cross-reactivity of human autoantigenic peptides and to further evaluate the specificity and safety of SCG101 epitope recognition. Computer-based prediction of a human-derived peptide library based on amino acids at positions 3 to 6 was performed by a bioinformatics algorithm

873 (http://webclu.bio.wzw.tum.de/expitope2/) to predict similar peptides and their potential
874 presentation by the HLA allele of interest. Nine peptides were found to contain four key amino
875 acids consistent with S20-28. To expand the cross-reactivity testing, we further obtained 14
876 peptide sequences from the database with at least six amino acids identical to the S20-28 peptide
877 by computer-based prediction (http://webclu.bio.wzw.tum.de/expitope2/). No peptide in the
878 human peptide library was found to have more than six amino acid sites consistent with the
879 S20-28 peptide. The 23 artificially synthesized peptides were assayed by T2 cells separately
880 loaded with different concentrations of peptides and co-incubated with SCG101 to detect
881 cytokine secretion.
882
883 **Xenograft models**
884 Mouse experiments were performed in a facility accredited by the Association for Assessment
885 and Accreditation of Laboratory Animal Care International (AAALAC). The Institutional
886 Animal Care and Use Committee (IACUC) approved the procedures used in this study under
887 IACUC serial number ACU21 -691 / -1064 / -1168. NOD-Cg-PrkdcSCIDIL-2Rgcnull/vst
888 (NPG, Beijing Vitalstar Biotechnology Co., Ltd.) mice (female:male= 1:1) were
889 subcutaneously inoculated with 1×10^7 tumor cells/animal in the right armpit. Six days after
890 inoculation, 60 animals were divided into six groups according to tumor volume and body
891 weight for the following groups: vehicle group (containing CS10 (BioLife Solutions, Inc.), HSA
892 (Baxalta US Inc.) and sodium chloride (Hunan Kelun Pharmaceutical Co., Ltd.) at a ratio of
893 50:5:45 (V:V:V)), untransduced (UT) cells control group (4.3×10^7 total T cells/animal),
894 SCG101 very low dose group (0.2×10^7 TCR-T cells/animal), SCG101 low dose group (0.5×10^7
895 TCR-T cells/animal), SCG101 moderate dose group (0.5×10^7 TCR-T cells/animal) and high
896 dose group (2.0×10^7 TCR-T cells/animal). All mice were dosed once by intravenous infusion
897 into the tail vein with a volume of 400 μl, and the first day of dosing was defined as D0. Body
898 weight and tumor volume measurements were made twice before grouping and after dosing
899 twice weekly on D2, D5, D8, D11, D15, D18, D21. Vernier calipers were used to measure the
900 major axis and minor axis for calculation of the tumor volume (V) according to the formula:
901 $V(mm^3) = 1/2\times$major axis (mm)$\times$minor axis $(mm)^2$. GraphPad Prism (8.0) software was used to
902 analyze dynamic parameters such as body weight and tumor volume by a two-way analysis of

903 variance. If ANOVA showed statistical significance ($p<0.05$), a Bonferroni post-test was
904 performed for multiple comparisons.
905
906 **Patient and AE monitoring**
907 All AE were graded according to the Common Terminology Criteria for Adverse Events (CTC
908 AE) version 5.0. Cytokine release syndrome (CRS) and Immune effector cell-associated
909 neurotoxicity syndrome (ICANS) were assessed and graded using the American Society for
910 Transplantation and Cellular Therapy (ASTCT) grading. Dose-limiting toxicities (DLTs) were
911 to be observed within 28 days post cell infusion, and DLTs were to be reviewed by a Safety
912 Review Committee.
913 Blood samples were collected and then analyzed by the clinical chemistry and diagnostics
914 department of the Peking Union Medical College Hospital to monitor CRS, key organ function
915 changes, and pharmacodynamic signals frequently. Serum liver function was tested at the
916 screening visit and baseline visits before leukapheresis and before lymphodepletion,
917 respectively, and on D-1, D1, D2, D4, D5, D7, D10, D14, D17, D21, D28, M2, and every two
918 months afterward; Serum biochemistry was tested at the screening visit, and at baseline visits
919 before leukapheresis and before lymphodepletion, respectively, and on D-1, D4, D7, D14, D21,
920 D28, M2, and every two months afterward; Hematological parameters were tested at the
921 screening visit, and at baseline visits before leukapheresis and before lymphodepletion,
922 respectively, every day within 14 days post cell infusion, and on D21, D28, M2, and every two
923 months afterward; Cytokine panel and serum HBsAg were tested on D-1, D1, D7, D14, D21,
924 D28, M2, and every two months afterward. Ferritin and CRP were tested every day within 14
925 days post cell infusion.
926
927 **SCG101 monitoring in peripheral blood**
928 The clinical blood samples were treated with hemolysin to lyse red blood cells and then stained
929 as described above. CountBright™ Plus Absolute Counting Beads (ThermoFisher) were added,
930 thoroughly mixed, and analyzed by the following equation to calculate the absolute lymphocyte
931 count (cells/L):
932 (cell count/counting beads count)x(total beads count/blood volume)

Based on this result, the SCG101 TCR-T cell concentration in peripheral blood was calculated with the following formula:

Absolute lymphocyte count×($CD3^+$cells/lymphocytes)×(TCR-T cells/$CD3^+$ cells).

Additionally, the vector copy number (VCN) was measured to quantify the persistence of SCG101 cells in peripheral blood. For this, the woodchuck hepatitis post-transcriptional regulatory element region of the lentiviral transgene was detected by qPCR. Patient samples of 2 ml of peripheral blood were collected on D-1, D2, D4, D7, D10, D14, D17, D21, D28, M2, and every two months afterward. gDNA was extracted using the QIAamp DNA Midi Kit (Qiagen). The standard curve for the transcript copy number was established by amplifying a ten-fold serially diluted linearized plasmid. The number of transgene copies per microgram of gDNA was determined on a QuantStudio™ 5 (Thermo Fisher Scientific) triplicated for each sample. The limit of detection of this assay was 100 copies per microgram of gDNA.

Supplementary References

1. Wisskirchen K, Metzger K, Schreiber S, Asen T, Weigand L, Dargel C, et al. Isolation and functional characterization of hepatitis B virus-specific T-cell receptors as new tools for experimental and clinical use. Plos One. 2017;12:e0182936.

2. Sommermeyer D, Uckert W. Minimal Amino Acid Exchange in Human TCR Constant Regions Fosters Improved Function of TCR Gene-Modified T Cells. J Immunol. 2010;184:6223–31.

Supplementary Figures

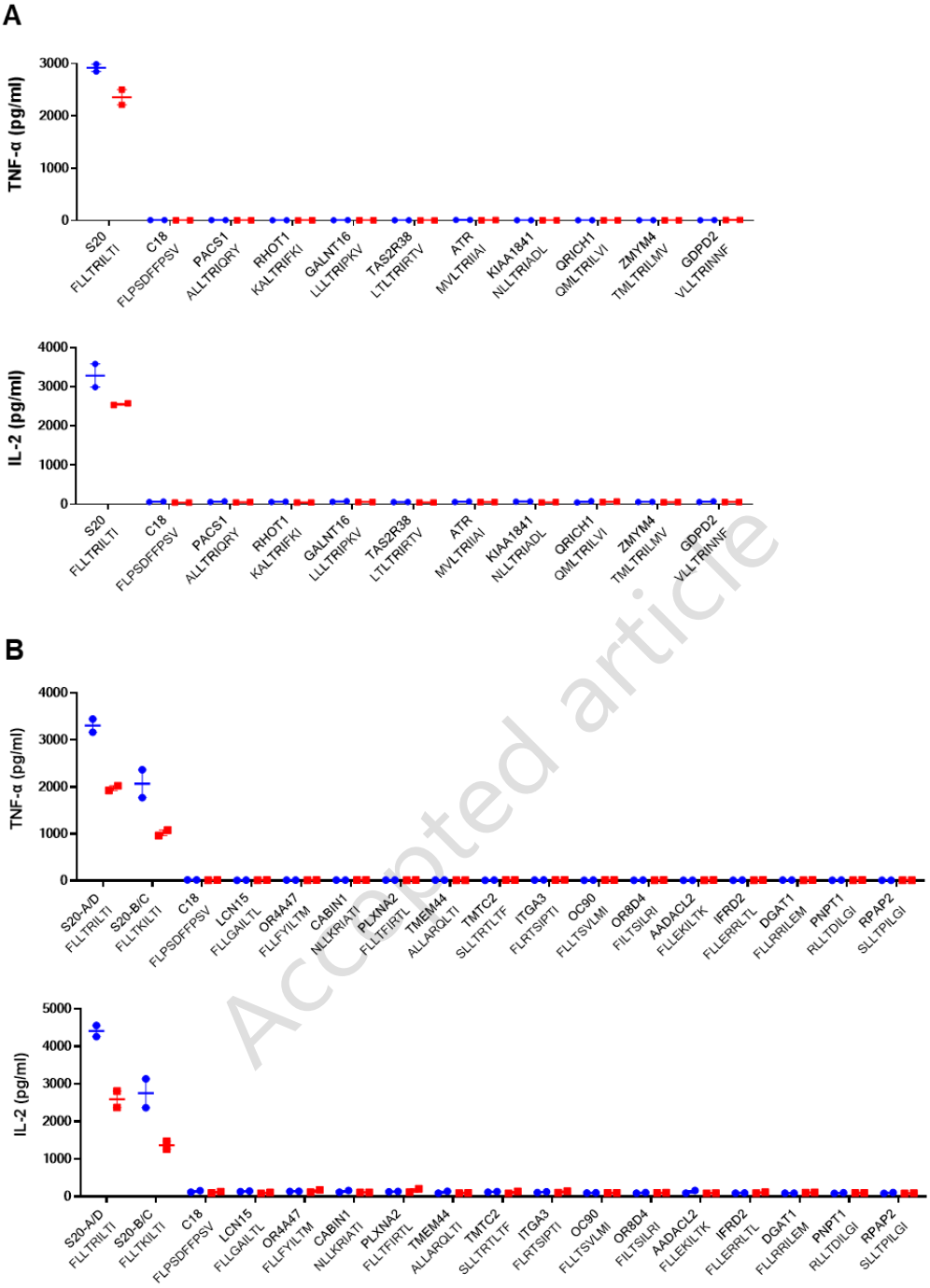

Supplementary Figure 1. Off-target analysis of SCG101.
T cells were co-cultured with T2 cells loaded with the indicated peptides and the supernatant was analyzed for TNF-a and IL-2 via CBA. **(A)** Cross-reactivity screening of SCG101 against human peptides containing the core binding motif L3 / T4 / R5 / I6 at concentrations of 1 (blue circles) and 0.1 (red squares) µg/ml. **(B)** Cross-reactivity of SCG101 against human peptides containing ≥ six amino acid sites consistent with the S20 peptide. S20 peptide FLLTKILTI represents a variant often found in HBV genotypes B and C. Mean values of duplicates are shown. The labeling indicates the name of the human gene containing the respective peptide sequence.

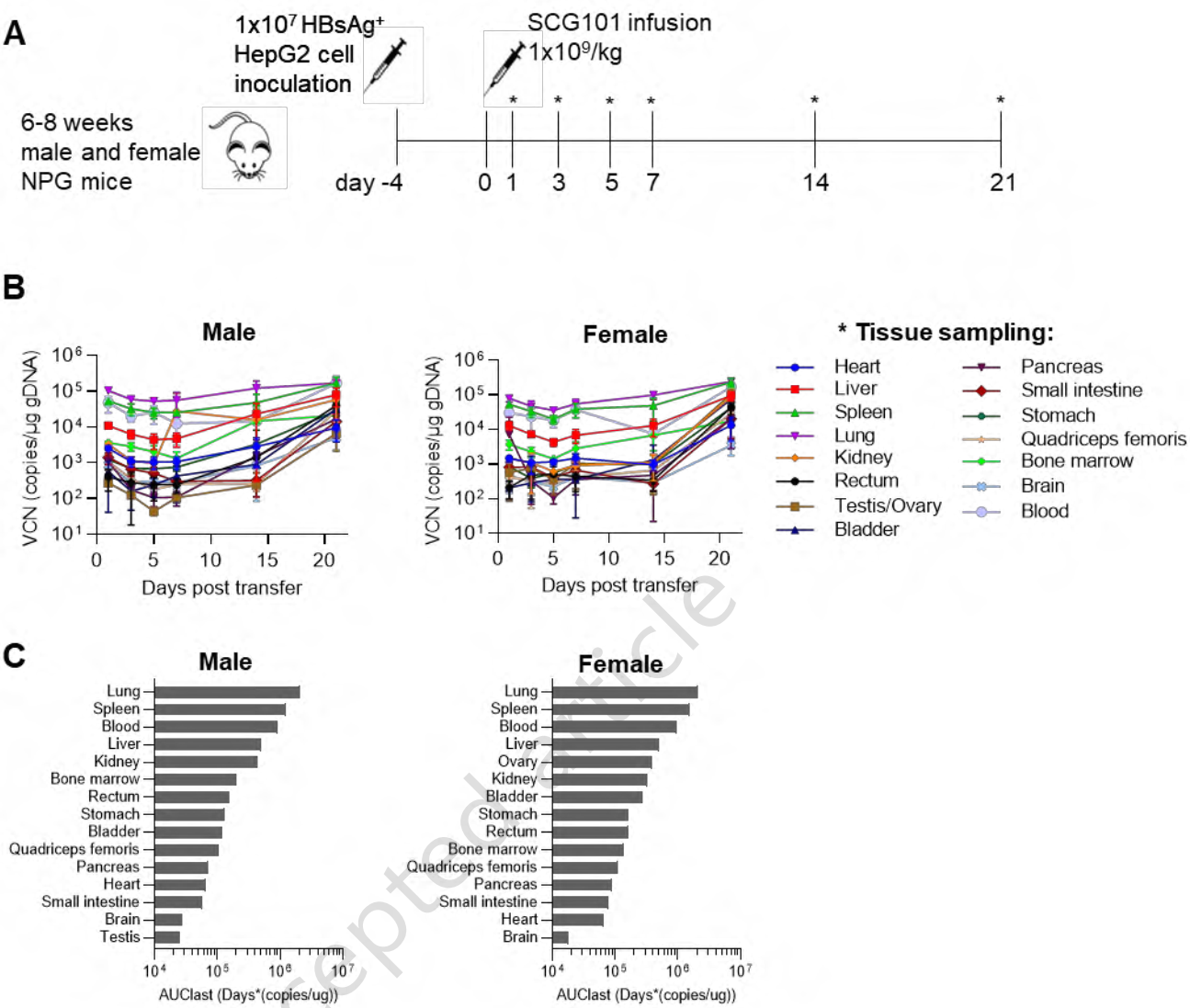

Supplementary Figure 2. Preclinical tissue distribution of HBV-specific SCG101 T cells. **(A)** Sixty NOD-Cg.PrkdcSCID IL-2Rgcnull/vst (NPG) mice (female: male = 1:1) were subcutaneously inoculated with $1x10^7$ HBsAg+ hepatoma cells/animal in the right armpit. Four days after inoculation, mice received a single dose of $1x10^9$ multimer-positive TCR-T cells per kg (i.e. around $2x10^7$/20g) intravenously. Tissue samples from the heart, liver, spleen, lung, kidney, rectum, gonad (female: ovary, male: testis), bladder, pancreas, small intestine, stomach, quadriceps femoris, bone marrow, and brain were collected from ten animals on six different time points (indicated with *). **(B)** At each collection time point, DNA was extracted from the indicated tissues and analyzed for the copy numbers of the SCG101 vector integrates by quantitative PCR. Mean±SEM of n=10 per group (5 male, 5 female) are shown. **(C)** For each tissue, the area under the curve over all analysis time points was summarized for each gender separately.

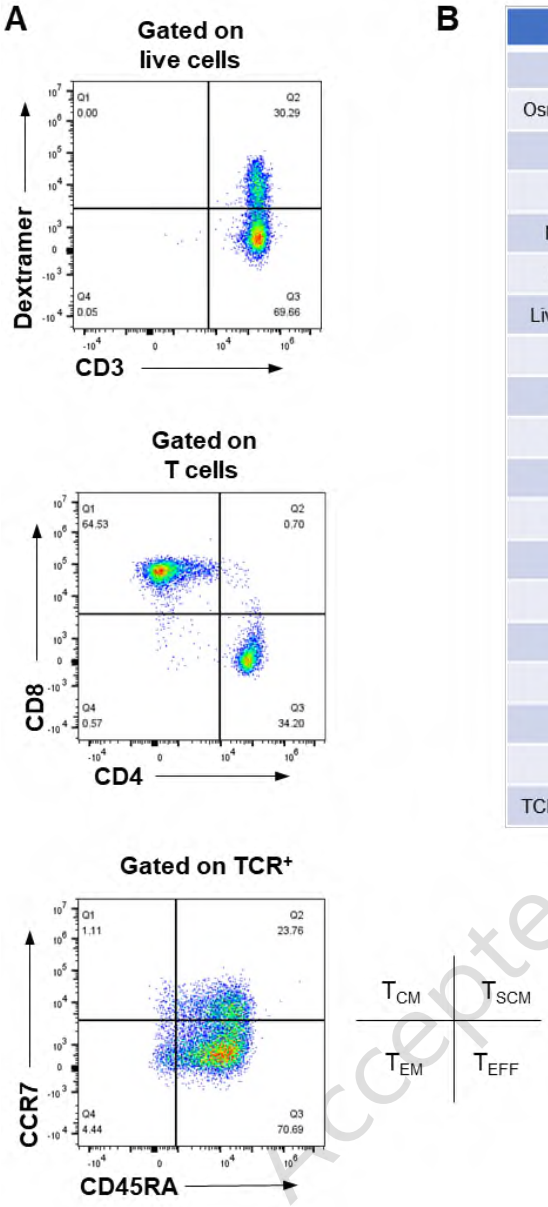

B

Test Items	Reference standard	Results
PH	6.50~8.00	6.61
Osmotic pressure	800~2000 mOsmol/Kg	1262 mOsmol/Kg
Sterility	Negative	Negative
Endotoxin	＜1.0 EU/mL	＜0.6 EU/mL
Mycoplasma	Negative	Negative
Cell viability	≥70.0%	87.0%
Live cell density	3.50×10^{7} ~6.50×10^{7} cells/mL	8.25×10^{7}cells/mL
Potency	E:T=1:2 cytotoxicity≥20%	83%
TCR+ rate	≥20.0%	30.32%
T cell ratio	≥90.0%	99.90%
Th ratio	N.A.	36.78%
CTL ratio	N.A.	62.12%
Ne ratio	≤5.00%	Not detectable
Mo ratio	≤5.00%	Not detectable
B ratio	≤5.00%	Not detectable
NK ratio	≤5.00%	Not detectable
VCN	≤ 10.00 copies/TCR^{+} cell	4.84 copies/ TCR^{+} cell
RCL	Negative	Negative
TCR identification	Positive	Positive

Supplementary Figure 3. SCG101 product release before infusion.

(A) Flow cytometry analysis of the clinical cell product via anti-CD3 and HBV S20-dextramer staining, composition of T cell subsets with anti-CD8 and anti-CD4 staining, and memory differentiation status with anti-CCR7 and anti-CD45RA staining. **(B)** Quality controls and release criteria before infusion. Th (T helper), CTL (cytotoxic T lymphocyte), Ne (Neutrophil), Mo (Monocyte), VCN (virus copy number), RCL (replication-competent lentivirus).

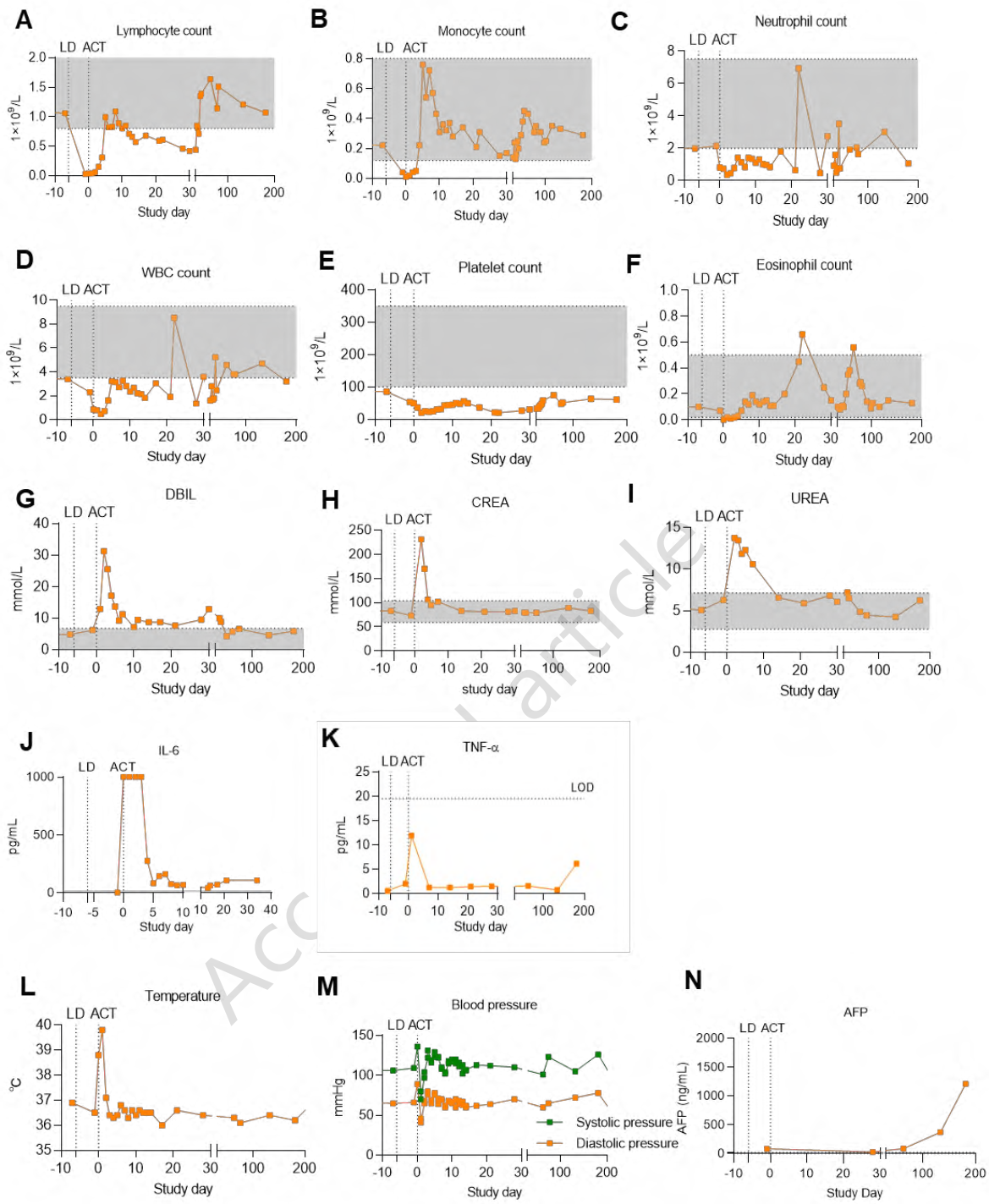

Supplementary Figure 4. Changes in serum markers after transfer of SCG101 HBV-specific T cells. (A-N) All clinical parameters that changed after infusion of SCG101 are shown. Blood cells were quantified via electrical impedance in the hospital and values might differ from flow cytometry results shown in figure 6. In addition, other clinical parameters in hematology, serum biochemistry, coagulation, and urinalysis were also tested regularly and did not show any significant changes during the observation period. The normal range is indicated by a grey area. LOD: limit of detection. **(J)** IL-6 detected by the diagnostic assay in the hospital reached a value above the upper detection limit of 1000 pg/ml. **(L,M)** Temperature and blood pressure measured daily for two weeks after adoptive cell transfer. LD= lymphodepletion, ACT= adoptive cell transfer.

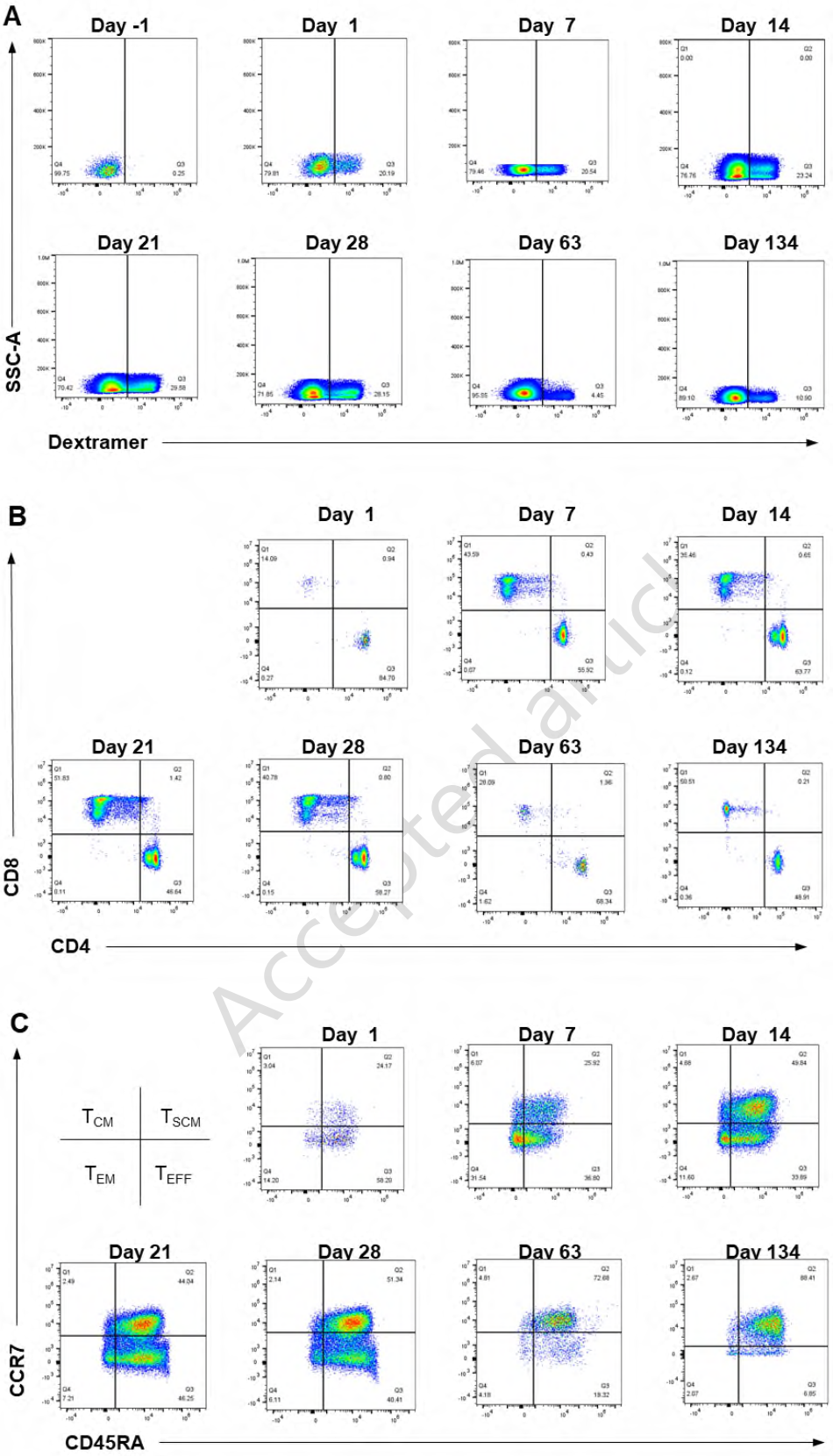

Supplementary Figure 5. Time course of flow cytometry of blood samples after T cell transfer. (A) Dextramer staining, **(B)** CD8 and CD4 distribution, **(C)** memory phenotype at indicated time points. The gating strategy is shown in main Figure 6A.